PB85-200020

Temporal and Spatial Variability of the Visual Effects of Stack Plumes

Systems Applications, Inc., San Rafael, CA

Prepared for

Environmental Protection Agency
Research Triangle Park, NC

May 85

U.S. Department of Commerce
National Technical Information Service
NTIS

PB85-200020

EPA/600/3-85/039
May 1985

TEMPORAL AND SPATIAL VARIABILITY OF THE VISUAL EFFECTS OF STACK PLUMES

by

Christian Seigneur
A. Belle Hudischewskyj
Henry Hogo

Systems Applications, Inc.
101 Lucas Vally Road
San Rafael, California 94903

P.O. 4D2173NASA

Project Officer

William D. Conner
Emission Measurement and Characterization Division
Atmospheric Sciences Research Laboratory
Research Triangle Park, North Carolina 27711

ATMOSPHERIC SCIENCES RESEARCH LABORATORY
OFFICE OF RESEARCH AND DEVELOPMENT
U.S. ENVIRONMENTAL PROTECTION AGENCY
RESEARCH TRIANGLE PARK, NORTH CAROLINA 27711

TECHNICAL REPORT DATA (Please read Instructions on the reverse before completing)		
1. REPORT NO. EPA/600/3-85/039	2.	3. RECIPIENT'S ACCESSION NO. PB85 200020/AS
4. TITLE AND SUBTITLE TEMPORAL AND SPATIAL VARIABILITY OF THE VISUAL EFFECTS OF STACK PLUMES		5. REPORT DATE May 1985 6. PERFORMING ORGANIZATION CODE
7. AUTHOR(S) Christian Seigneur, Belle Hudischewskyj and Henry Hogo		8. PERFORMING ORGANIZATION REPORT NO.
9. PERFORMING ORGANIZATION NAME AND ADDRESS Systems Applications, Inc. 101 Lucas Valley Road San Rafael, CA 94903		10. PROGRAM ELEMENT NO. CDTA1D/10-4051 (FY-85) 11. CONTRACT/GRANT NO. P.O. 4D2173NASA
12. SPONSORING AGENCY NAME AND ADDRESS Atmospheric Sciences Research Laboratory - RTP, NC Office of Research and Development U.S. Environmental Protection Agency Research Triangle Park, North Carolina 27711		13. TYPE OF REPORT AND PERIOD COVERED Final 2/1/83 to 1/1/84 14. SPONSORING AGENCY CODE EPA/600/09
15. SUPPLEMENTARY NOTES		

16. ABSTRACT

Temporal and spatial variabilities of stack plumes are analyzed by means of field data analysis and computer simulations. In this investigation, photographs from field programs of the study Visibility Impairment due to Sulfur Transport and Transformation in the Atmosphere were analyzed via sensitometry, and PLUVUE II model simulations were conducted for a case study. Analysis of the temporal variability of plume visibility led to documentation of the fact that the visual effects of plumes vary with time because of (1) turbulent fluctuations, (2) changes in atmospheric stability, and (3) changes in the observer-plume-sun scattering angle. Likewise, the analysis of the spatial variability of plume visibility led to the fact that the visual effects of plumes vary with downwind distance from the stacks because of (1) turbulent fluctuations, (2) dilution of the plume and/or a change in the observer-plume distance, and (3) changes in the observer-plume-sun scattering angle.

17. KEY WORDS AND DOCUMENT ANALYSIS		
a. DESCRIPTORS	b. IDENTIFIERS/OPEN ENDED TERMS	c. COSATI Field/Group
18. DISTRIBUTION STATEMENT RELEASE TO PUBLIC	19. SECURITY CLASS (This Report) UNCLASSIFIED	21. NO. OF PAGES 50
	20. SECURITY CLASS (This page) UNCLASSIFIED	22. PRICE

EPA Form 2220-1 (Rev. 4-77) PREVIOUS EDITION IS OBSOLETE

DISCLAIMER

The information in this document has been funded wholly or in part by the United States Environmental Protection Agency under P.O. No. 4D2173NASA to Systems Applications, Inc. It has been subject to the Agency's peer and administration review, and it has been approved for publication as an EPA document. Mention of trade names or commercial products does not constitute endorsement or recommendation for use.

ABSTRACT

The impact of chimney plumes on atmospheric visibility has been the subject of extensive experimental and theoretical studies such as those performed in the comprehensive VISTTA research program. An important conclusion of these plume-visibility studies was that there is a major discrepancy between the nature of the measurements of plume visibility and computer simulations of plume visibility. This discrepancy occurs because measurements are conducted over short time intervals (teleradiometric) or even instantaneously (photographic), whereas simulations assume steady-state conditions. Thus, the temporal and spatial variability of plume visibility effects must be considered when evaluating plume visibility models with atmospheric data and when applying these plume visibility models in a regulatory context.

We analyzed the temporal and spatial variability of stack plumes by means of field data analysis and computer simulations. Photographs from the VISTTA field programs were analyzed via sensitometry, and PLUVUE II model simulations were conducted for a case study.

Our analysis of the temporal variability of plume visibility documents the fact that the visual effects of plumes vary with time because of (1) turbulent fluctuations, (2) changes in atmospheric stability, and (3) changes in the observer-plume-sun scattering angle.

Our analysis of the spatial variability of plume visibility documents the fact that the visual effects of plumes vary with downwind distance from the stacks because of (1) turbulent fluctuations, (2) dilution of the plume and/or increase/decrease in the observer/plume distance, and (3) changes in the observer-plume-sun scattering angle.

CONTENTS

Abstract..... iii

Figures..... vi

Tables..... viii

Acknowledgment..... ix

1 Introduction..... 1

2 Conclusions..... 3

3 Data Base and Experimental Procedure..... 5

4 Temporal Variability of Plume Visibility..... 14

5 Spatial Variability of Plume Visibility..... 26

References..... 38

FIGURES

Number		Page
1	Example of sensitometric measurements.....	7
2	Navajo power plant plume. 7 December 1979 (Kaibito Plateau site).....	15
3	Navajo power plant plume. 7 December 1979, (Lechee Rock site).....	16
4	Navajo power plant plume. 15 December 1979.....	17
5	Kincaid power plant plume. 20 February 1981.....	18
6	Kincaid power plant plume. 24 February 1981 (right side of slide).....	19
7	Kincaid power plant plume. 24 February 1981 (left side of slide).....	20
8	Model simulation of the Kincaid power plant plume. 24 February 1981 (right side of slide).....	22
9	Model simulation of the Kincaid power plant plume. 24 February 1981 (left side of slide).....	23
10	Navajo power plant plume. 1200 LST. 7 December 1979.....	27
11	Navajo power plant plume. 0905 LST. 15 December 1979.....	28
12	Kincaid power plant plume. 1117 LST. 20 February 1981.....	29
13	Kincaid power plant plume. 0951 LST. 24 February 1981.....	31
14	Model simulation of the Kincaid power plant plume. 0951 LST. 24 February 1981.....	32

Number		Page
15	Model simulation of the Kincaid power plant plume. 0951 LST. 24 February 1981. Wind direction = 340°.....	34
16	Model simulation of the Kincaid power plant plume. 0951 LST. 24 February 1981. Mean radius of coarse aerosols = 5 μm.....	35

TABLES

Number		Page
1	Slides selected for the temporal variability analysis.....	12
2	Slides selected for the spatial variability analysis.....	13
3	Comparison of measured and calculated plume/sky radiance ratios for the Kincaid power plant plume, 0814 LST, 24 February 1981.....	37

ACKNOWLEDGMENT

We thank Dr. William E. Wilson and Mr. William D. Conner for providing continuous support throughout the course of this study. We also thank Ms. Judy A. Rodich for editing this final report.

1 INTRODUCTION

The impact of stack plumes on atmospheric visibility has been the subject of extensive experimental and theoretical studies over the past five years. Of these studies, the Visibility Impairment due to Sulfur Transport and Transformation in the Atmosphere (VISTTA) program appears to be the most comprehensive research effort conducted to investigate the chemistry, physics, and optics of stack plumes as they relate to impacts on atmospheric visibility. The VISTTA program comprised four field programs conducted in 1979 and 1981 as well as an evaluation of the EPA plume visibility models PLUVUE and PLUVUE II.

The major findings of the 1979 field programs have been presented by Richards et al. (1981) and Blumenthal et al. (1981), and those of the 1981 field program by Richards et al. (in press) and Seigneur et al. (1984b). Evaluation of the visibility model PLUVUE with the 1979 VISTTA data has been presented by Bergstrom et al. (1981) and White et al. (in press); evaluation of the visibility model PLUVUE II with the 1981 VISTTA data has been presented by Seigneur et al. (1984b).

An important conclusion of these plume-visibility studies was that there is a major discrepancy between the nature of the measurements of plume visibility and computer simulations of plume visibility. Measurements of plume visibility were taken over a given time interval (about 15 to 30 minutes for teleradiometer measurements, and instantaneous measurements for the sensitometry of color slides) and at a given location. Fluctuations caused by atmospheric turbulence lead to plume visibility effects that vary with time and location. Simulations of plume visibility, on the other hand, were conducted with mathematical models that assume steady-state conditions, a given atmospheric stability class, and time-averaged dispersion coefficients. The discrepancy between the time-and-location-specific nature of measurements and the time-averaged (e.g., dispersion coefficients) and conditions-averaged (e.g., atmospheric stability) nature of model simulations results necessarily in differences between experimental measurements and model simulations.

White et al. (in press) estimated the uncertainties that result from the turbulent fluctuations of the atmosphere in their comparison of model simulation results with data from the 1979 VISTTA experimental results.

In this study, we investigate the temporal and spatial variability of plume visibility in a systematic fashion. We analyze a series of color slides from the 1979 and 1981 VISTTA field programs by means of sensitometry to determine the temporal and spatial variability of plume visual effects. Conclusions can thus be drawn about the uncertainties that will result when using atmospheric data on plume visibility for model evaluation.

Another area of uncertainty in comparing model calculations with atmospheric data is the accuracy of specific experimental data, such as, for example, NO_2 plume concentrations and aerosol size distributions. This source of uncertainty is also partially investigated in this study when we compare model simulation results with experimental data. Because largest uncertainties appear to be associated with the calculation of the visual effects of plumes for forward scattering conditions, we focus on the effect of aerosol size distributions and scattering angle on plume visibility for such conditions.

Section 2 provides an overview of the data base that was used in this study as well as the data processing. Section 3 presents the results of an analysis of the temporal variability of plume visibility. Section 4 presents the results of analyses of the spatial variability of plume visibility. The sensitivity analysis of plume model calculations for bright plumes is also presented in Section 4. Section 5 summarizes the findings of this study.

2 CONCLUSIONS

We have investigated the temporal and spatial variability of stack plumes by means of field data analysis and computer simulations. A series of 46 photographs of plumes from the Navajo (Arizona) and Kincaid (Illinois) power plant plumes taken during the VISTTA field programs was digitized, and a sensitometric analysis provided the values of the plume/sky radiance ratios at three wavelengths 650 (red), 550 (green), and 450 (blue) nm. These photographs were taken on 7 December (from two different sites) and 15 December 1979 for the Navajo power plant plume and on 20 and 24 February 1981 for the Kincaid power plant plume. Model simulations of plume visibility were conducted for the Kincaid power plant plume observed on 24 February 1981.

Our analysis of the temporal variability of plume visibility suggests that the visual effects of plumes vary with time because of several factors.

(1) Turbulent fluctuations lead to random variations in plume visibility; this phenomenon was observed for the Navajo power plant plume on 7 December 1979.

(2) An evolution of atmospheric stability toward more unstable conditions from early morning to mid-afternoon leads to a more dilute and less visible plume; this effect was observed for the Navajo power plant plume on 15 December 1979 and the Kincaid power plant plume on 20 February 1981.

(3) A change in the observer-plume-sun scattering angle due to the change in the sun's location leads to variations in plume visual effects; this phenomenon was observed in model simulations and possibly in measurements of the Kincaid power plant plume on 24 February 1981.

Our analysis of the spatial variability of plume visibility suggests that the visual effects of plumes vary with downwind distance from the stacks because of the following factors:

(1) Turbulent fluctuations lead to random variations in plume visibility; this phenomenon was more evident in observations of the Kincaid power plant plume on 20 February 1981.

(2) Dilution of the plume and/or increase in the observer/plume distance lead to a decrease in plume visibility; this effect was observed in the Navajo power plant plume on 7 and 15 December 1979.

(3) A change in the observer-plume-sun scattering angle may lead to a variation in plume visual effects (e.g., from bright to dark); this effect was observed and, to a certain extent, simulated, for the Kincaid power plant plume on 24 February 1981.

3 DATA BASE AND EXPERIMENTAL PROCEDURE

The VISTTA visibility data base includes data collected near the Navajo power plant in June-July and December 1979, near the Kincaid power plant in February 1981 and near the Labadie power plant and San Manuel smelter in August-September 1981. For this study, it was necessary to select color slides of power plant or smelter plumes that would constitute a time series of a given plume so that the temporal variability of plume visibility could be analyzed. To study spatial variability, any color slide of a discernible plume would be appropriate; however, we restricted our analysis of spatial variability to slides that had already been selected for the temporal variability analysis. We thus maintained the consistency of these two complementary analyses while reducing the experimental cost of data processing.

On the basis of these considerations, the slides utilized in this study were selected from the December 1979 program at the Navajo power plant and from the February 1981 program at the Kincaid power plant. These slides offered the best time series of the visual effects of stack plumes collected during the four VISTTA field programs. A total of 46 slides were chosen for sensitometric analysis (i.e., digitization). These 46 slides represented plume visual effects observed on 7 and 15 December 1979 at the Navajo power plant (24 color slides) and on 12, 20, 24, and 25 February 1981 at the Kincaid power plant (16 slides). Six color slides of the reference gray color charts were also included.

These slides were digitized at Perkin-Elmer in Garden Grove, California. For the temporal variability analysis, each slide was processed at a given location. The section of the photograph to be digitized corresponded to an imaginary vertical line across the plume so that both the background below and above the plume and the plume itself were digitized. The procedure is therefore similar to the vertical scan taken with a teleradiometer. Since there may be some uncertainty regarding the exact location of such a scan due to spatial variability of the picture elements (pixels), three digital scans, 35 μm apart horizontally, were performed on the slides. An average of these three scans was used in the data analysis.

For the spatial variability analysis, five slides were selected from 7 and 15 December 1979 (Navajo power plant) and 12, 20, and 24 February 1981 (Kincaid power plant). Series of 10 vertical scans were performed on these slides at equal horizontal intervals that covered the entire slide range. These scans corresponded to plume visibility measurements conducted at different downwind distances from the same observation site (i.e., the site where the photograph was taken).

The slide digitization process may be summarized as follows. The aperture used in the digitization process was 35 μm square. Smaller resolution, though possible, would result in a lower response of the photographic film; thus, the 35-μm-square aperture appeared to be the most appropriate (Eastman Kodak Company, 1974). This aperture corresponds to a vertical subtending angle of view of 0.039°, which is similar to the 0.035° angle of view of the teleradiometer.

The slide digitization was conducted at three wavelengths using narrow-band filters (Kodak Wratten filters numbers 92 [red], 93 [green], and 94 [blue]). Filter transmittance is above 0.1 percent between 420 and 500 nm (blue filter). Peak filter transmittance occurs at 450 nm (blue filter), 540 nm (green filter), and above 700 nm (red filter) (Eastman Kodak Company, 1976). The maximum sensitivities of the three layers of Kodachrome 64 film are at 430 nm (yellow-forming layer), 550 nm (magenta-forming layer), and 650 nm (cyan-forming layer) (Eastman Kodak Company, 1974).

An example of a series of slide-digitization scans using the three filters is shown in Figure 1 for slides taken on 15 December 1979 (Navajo power plant) and on 24 February 1981 (Kincaid power plant). The optical density of the pixels is plotted as a function of the vertical distance on the photographic scales for each of the three digital scans. It may be noted, however, that a higher density corresponds to a lower exposure so that a dark plume appears in a sensitometric plot as an increase in pixel density, whereas a bright plume appears as a decrease in pixel density.

The pixel density of the plume was defined as the value of the maximum (dark plume) or minimum (bright plume) of the plume section of the curves. The pixel density of the background sky at the same location was determined by interpolation between the sky density values below and above the plume. Average values were determined for these values since pixel densities were available for three scans.

The density of the pixels measured by the slide-digitization technique had to be converted into a quantity linearly related to the radiance that was recorded on the photographic slide. This conversion was achieved by using characterization curves that relate the slide density to the original

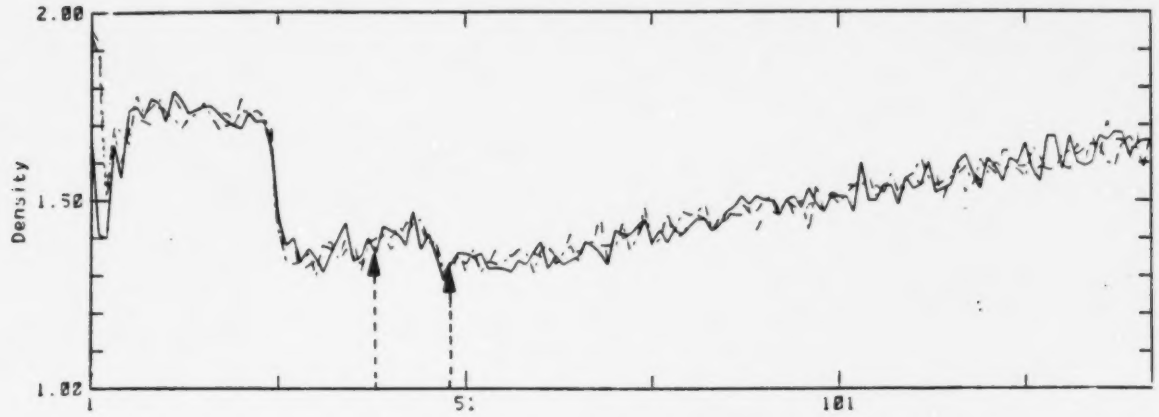

#11 RED

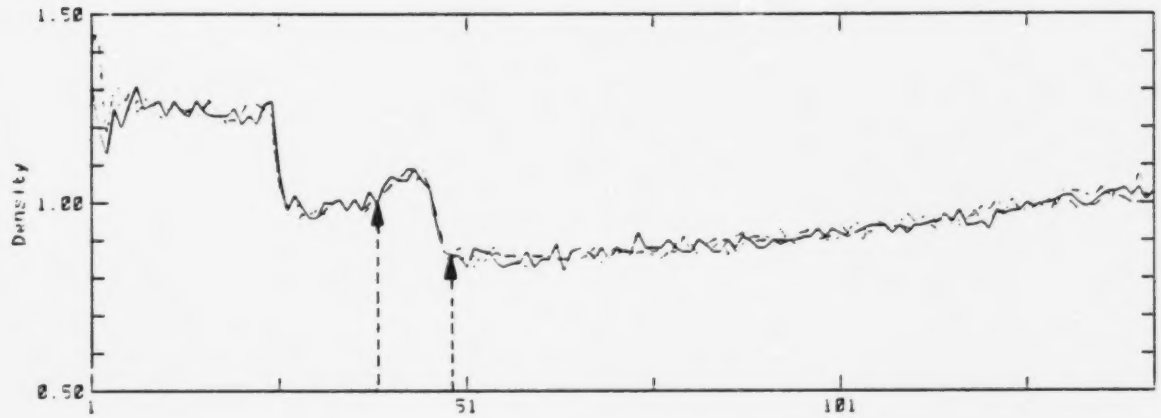

#11 GREEN

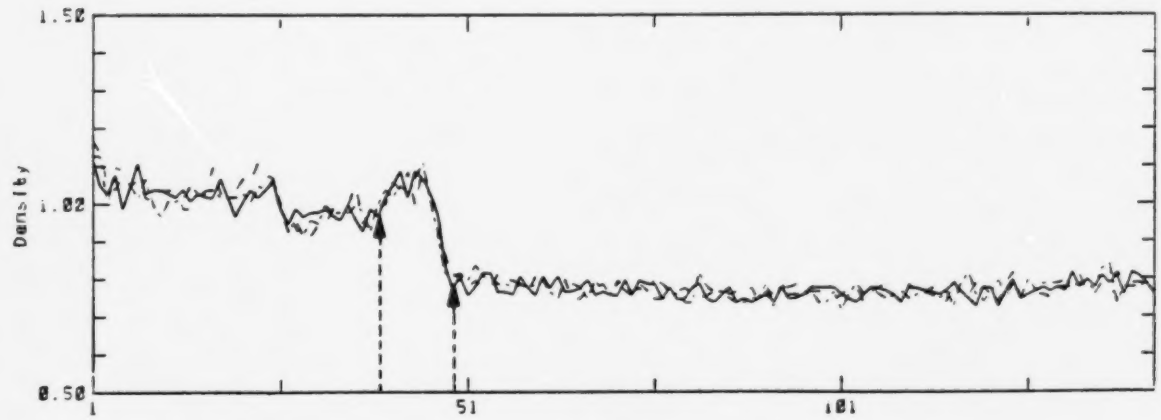

#11 BLUE

(a) Navajo power plant, 0825 LST, 15 December 1979.

FIGURE 1. Example of sensitometric measurements. Dashed vertical lines indicate the plume.

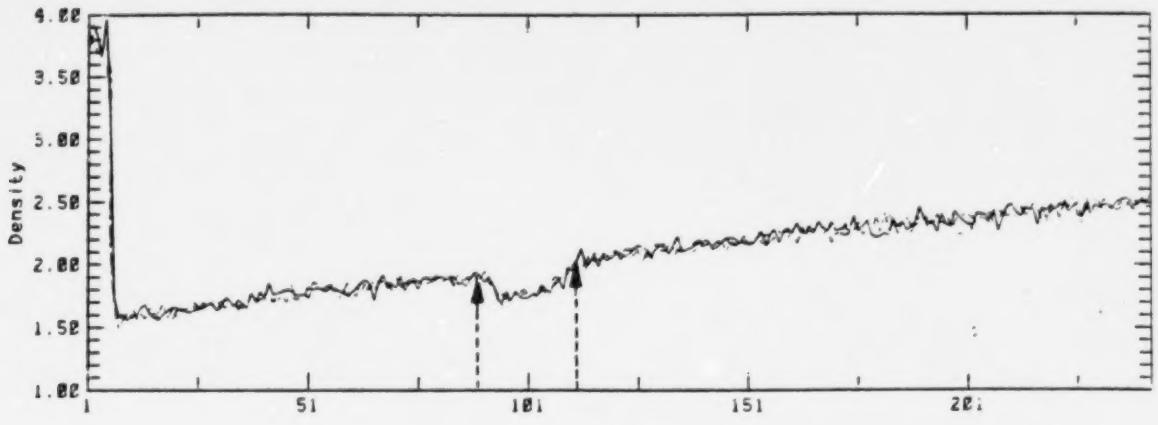

#37W RED

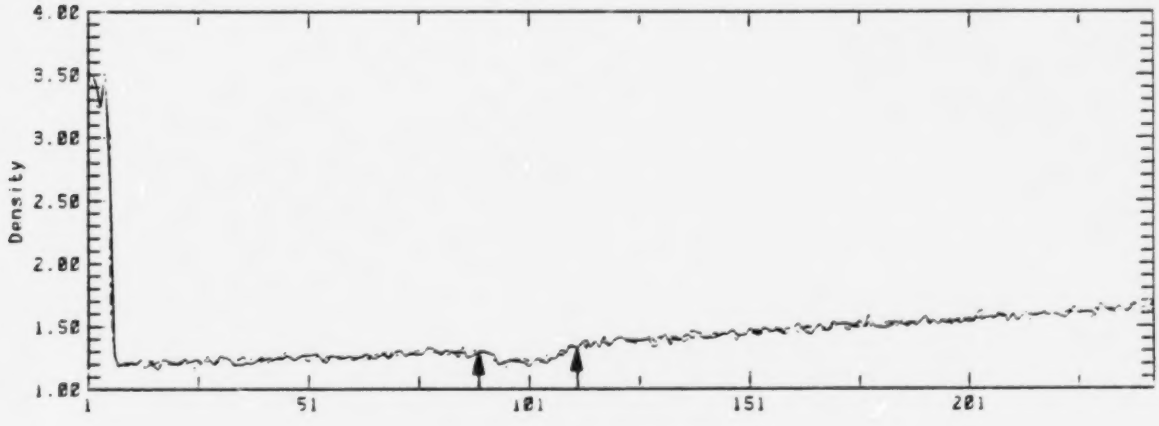

#37W GREEN

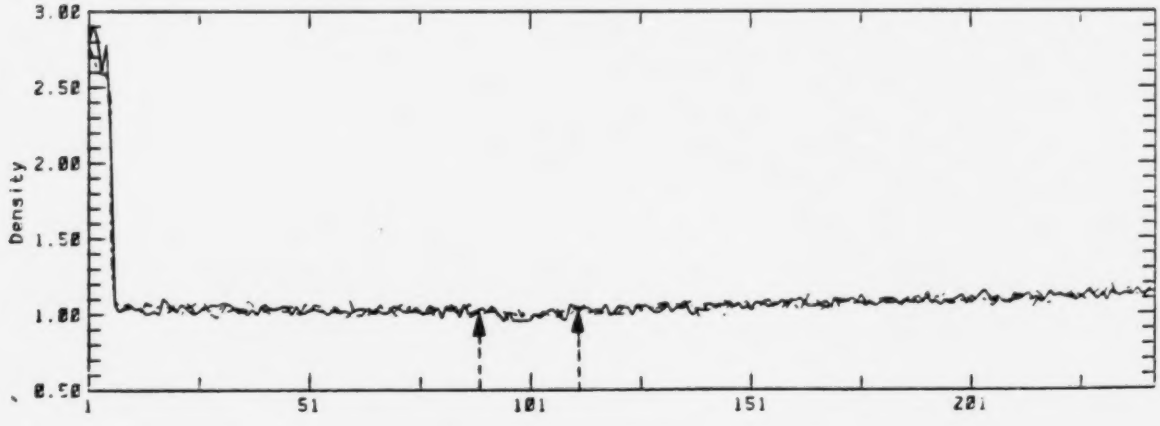

#37W BLUE

(b) Kincaid power plant plume, 0950 LST, 24 February 1981, right side of slide.

FIGURE 1 (continued).

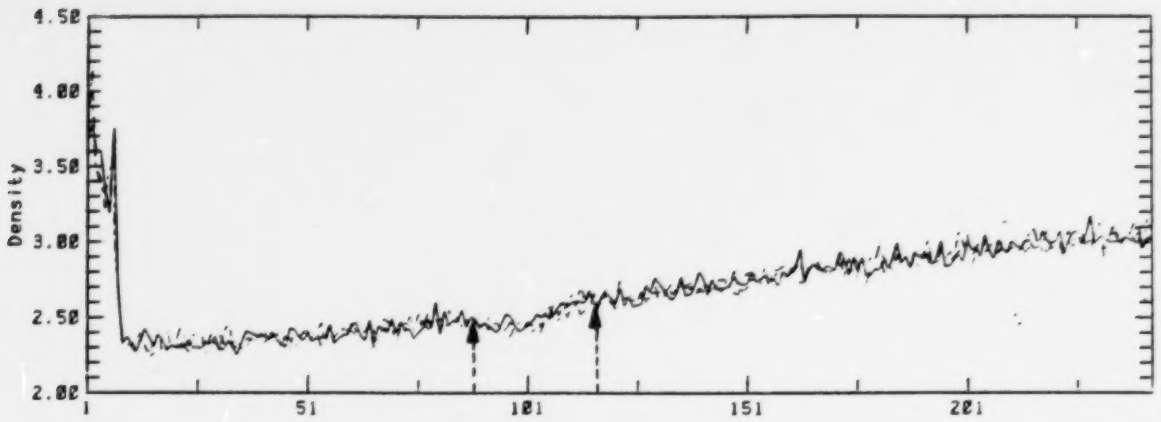

#37B RED

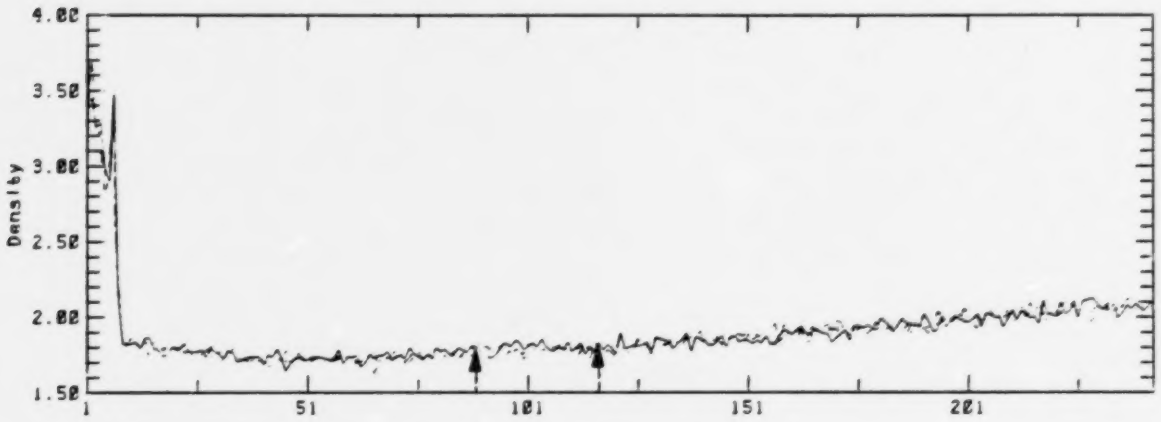

#37B GREEN

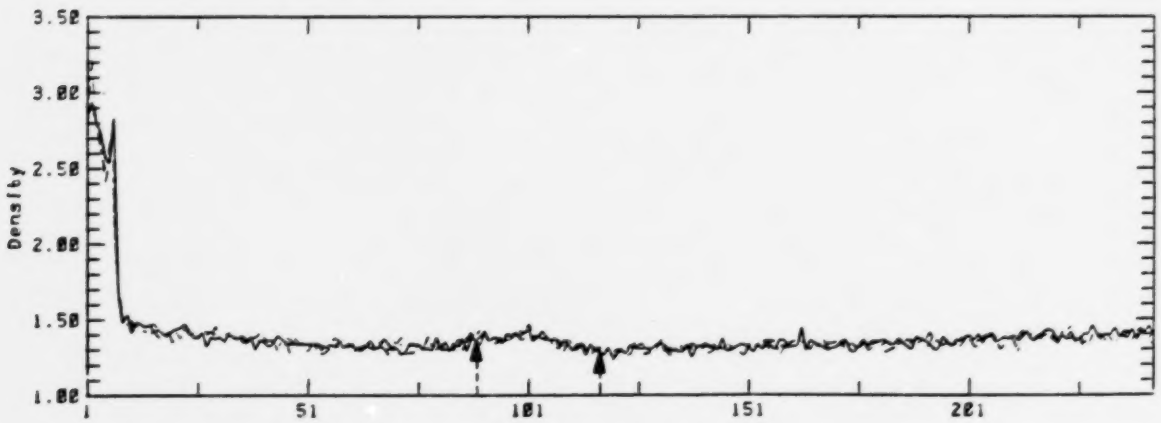

#37B BLUE

(c) Kincaid power plant plume, 0950 LST, 24 February 1981, left side of slide.

FIGURE 1 (concluded).

exposure for a given wavelength and exposure conditions. Standard characteristic curves are provided by Eastman Kodak Company (1974). However, it appears that the characteristic curves vary slightly from film to film and from one series of photographs to another because of different film pigment and exposure conditions. Therefore, it appeared to be more accurate to construct characteristic curves specific to the photographs being analyzed. These curves were constructed as follows: prior to photographic measurement of the plume, a reference gray scale placed perpendicular to the direct solar beam was photographed. Since reflectances of the gray scale were known (Macbeth, 1981), it was possible to construct a characteristic curve representing the pixel density as a function of a normalized exposure that was proportional to the gray scale reflectances. The use of a normalized exposure was suitable for this study because the sensitometric measurements are relative, that is, one measures the ratio of two radiances or a contrast. Differences between plume/sky radiance ratios calculated with characteristic curves constructed from a reference gray scale and radiance ratios calculated with standard characteristics curves (Eastman Kodak Company, 1974) ranged from 0 to 2 percent.

The pixel densities obtained from sensitometric curves were then converted to normalized exposures by means of the characteristic curves. A detailed description of this calculation is given elsewhere (Seigneur et al., 1984a).

Figure 1 presents typical densitometer scans of the Navajo and Kincaid power plant plumes. The Navajo power plant plume affects atmospheric visibility mainly through light absorption by NO_2 (Bergstrom et al., 1981; Richards et al., 1981; White et al., in press) and thus results in a dark plume that absorbs light mainly in the blue wavelengths. In Figure 1a, a clear bump appears in the blue wavelength scan between abscissae 30 and 50 on the horizontal scale. The effect of the plume is less pronounced at the green wavelength and is only slightly over the noise of the measurements at the red wavelength, where the optical effects result primarily from particle scattering. The large increase below abscissa 25 represents the background terrain below the plume.

The Kincaid power plant plume was visible primarily because of its scattering of light by particles (Seigneur et al., 1984b). Observation of this plume on 24 February 1981 revealed a particular geometry of scattering angles that leads to a bright appearance of the plume on the right side of the slide, where forward scattering predominates, and a dark appearance of the plume on the left side of the slide, where background scattering is more important. This difference appears clearly in Figures 1b and 1c. In Figure 1b, a slight hollow in the scan around abscissa 100 at the red wavelength characterizes the brightness of the plume due to

forward scattering of light. This effect is also slightly apparent at the green wavelength but is not evident at the blue wavelength. In Figure 1c, some brightness is still apparent at the red wavelength, but it is then overwhelmed by the backward scattering at the blue wavelength that appears as a bump around abscissa 100.

After processing of the digitized data, a review of the digitization scans was conducted to select the scans that could be analyzed, i.e., those for which a plume was discernible above the noise of the measurements. The list of slides selected for temporal variability analysis was reduced to 32. (The slides of 24 February 1981 were digitized at two different locations, one yielding a bright plume, and the other, a dark plume). Pertinent information about each slide is presented in Table 1. The list of slides selected for the study of spatial variability was reduced to 4 slides that are presented in Table 2.

TABLE 1. Slides selected for the temporal variability analysis.

Power Plant	Date	Time (LST)
Navajo	7 December 1979 (Kaibito Plateau)*	1145
	7 December 1979 (Kaibito Plateau)*	1200
	7 December 1979 (Kaibito Plateau)*	1210
	7 December 1979 (Kaibito Plateau)*	1215
	7 December 1979 (Kaibito Plateau)*	1245
	7 December 1979 (Kaibito Plateau)*	1300
	7 December 1979 (Kaibito Plateau)*	1330
	7 December 1979 (Kaibito Plateau)*	1345
Navajo	7 December 1979 (Lechee Rock)*	1025
	7 December 1979 (Lechee Rock)*	1037
	7 December 1979 (Lechee Rock)*	1101
	7 December 1979 (Lechee Rock)*	1137
	7 December 1979 (Lechee Rock)*	1147
	7 December 1979 (Lechee Rock)*	1205
	7 December 1979 (Lechee Rock)*	1225
	7 December 1979 (Lechee Rock)*	1239
Navajo	15 December 1979	0825
	15 December 1979	0850
	15 December 1979	0905
	15 December 1979	0930
	15 December 1979	1015
	15 December 1979	1050
	15 December 1979	1145
Kincaid	20 February 1981	1117
	20 February 1981	1147
	20 February 1981	1154
	20 February 1981	1212
	20 February 1981	1235
Kincaid	24 February 1981 (bright plume)†	0942
	24 February 1981 (bright plume)†	0951
	24 February 1981 (bright plume)†	1005
	24 February 1981 (bright plume)†	1024
Kincaid	24 February 1981 (dark plume)†	0942
	24 February 1981 (dark plume)†	0951
	24 February 1981 (dark plume)†	1005
	24 February 1981 (dark plume)†	1024

* Observation site. The two sites are approximately 24 km apart.
† Same plume and observation sites at different scattering angles.

TABLE 2. Slides selected for the spatial variability analysis.

Power Plant	Date	Time (LST)
Navajo	7 December 1979 (Kaibito Plateau)	1200
Navajo	15 December 1979	0905
Kincaid	20 February 1981	1117
Kincaid	24 February 1981	0951

4 TEMPORAL VARIABILITY OF PLUME VISIBILITY

The ratios of plume radiance to sky radiance were calculated by the sensitometric technique and plotted for each case study as a function of time. The results of these calculations are presented in Figures 2 through 7. The plume/sky radiance ratio is presented for three wavelengths--450, 550, and 650 nm. In Figure 3, the plume/sky radiance ratio at 650 nm could not be discerned from the pixel noise and is plotted as a value of 1 (i.e., no visual effect). Similarly, the plume/sky radiance ratio at 450 nm corresponds to the horizontal axis, i.e., a value of 1.

Figure 2 presents the plume/sky radiance ratio of the Navajo power plant plume observed from Kaibito Plateau on 7 December 1979 from 1145 LST to 1345 LST. Fairly large fluctuations are observed from 1145 to 1330 LST at all wavelengths. The darkest plume occurs at 1200 LST with a plume/sky radiance ratio of 0.7 at 450 nm. This ratio remains at approximately 0.8 until 1330 LST, when it falls to about 0.75. At 1345 LST, the plume is dispersed and no plume contrast is discernible, i.e., the plume/sky radiance ratio is equal to 1 at all three wavelengths. Seigneur et al. (1984a) estimated that the uncertainty in the plume/sky radiance ratio was about 4 percent for sensitometry. This value corresponds to a change of 0.03 for a ratio of 0.8 to 0.7. It appears, therefore, that the changes observed in the plume/sky radiance ratio on 7 December 1979 exceed the measurement uncertainties and reflect the variability of atmospheric parameters.

Figure 3 presents the results of observations of the Navajo power plant plume observed from Lechee Rock on 7 December 1979. No plume contrast was discernible in the red wavelengths. Notable variations occurred in the green and blue wavelengths between 1030 LST and 1240 LST. As in the previous case, these variations exceed the measurement uncertainties. Since there is no particular synchronism between the time series of Figures 2 and 3, the observers located at two different sites, Kaibito Plateau and Lechee Rock, were most likely sighting different portions of the plume.

Figure 4 presents the evolution of plume/sky radiance ratios of the Navajo power plant plume on 15 December 1979 from 1025 LST to 1145 LST. These results are a clear example of plume dispersion as atmospheric stability

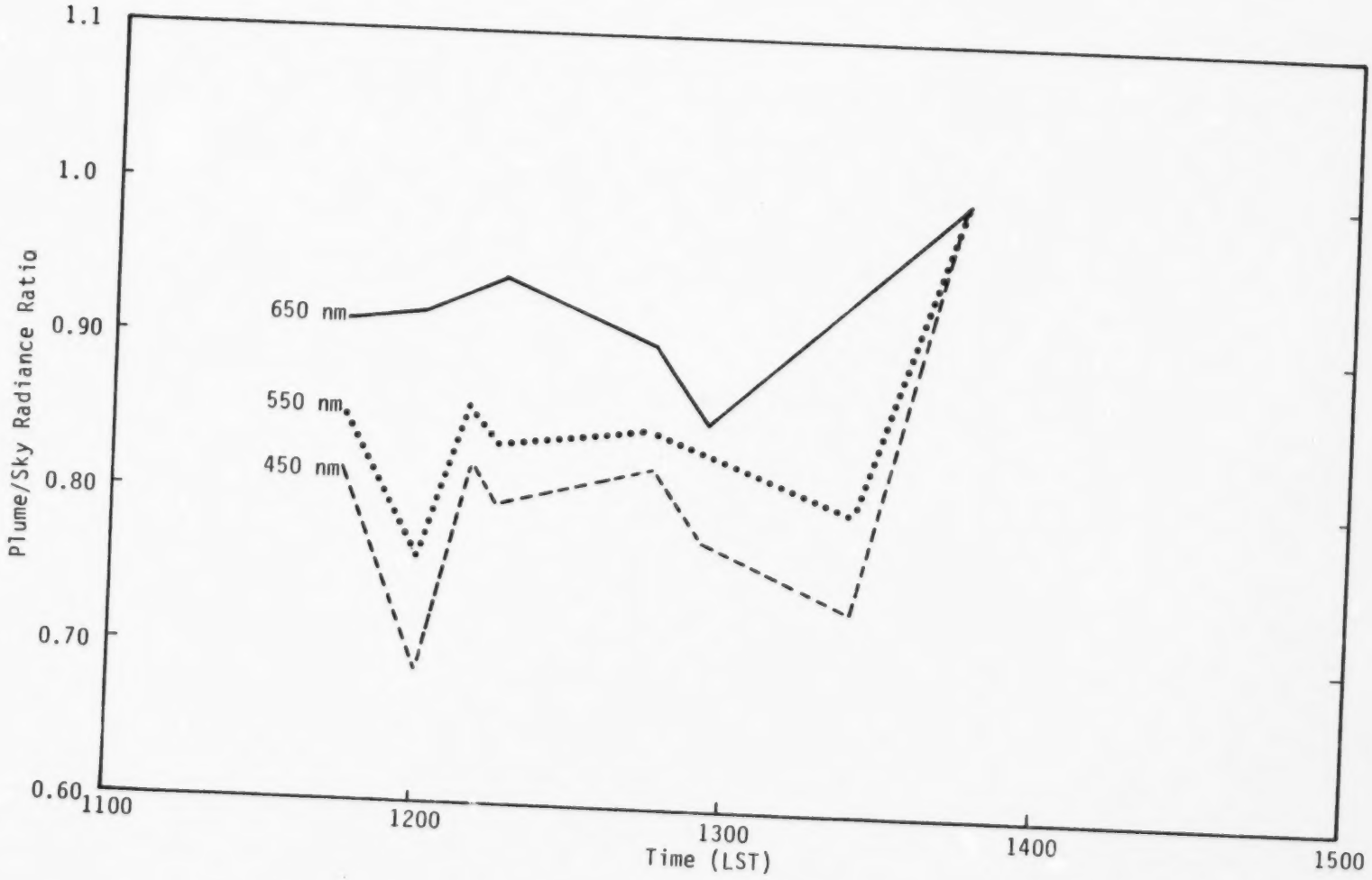

FIGURE 2. Navajo power plant plume. 7 December 1979 (Kaibito Plateau site).

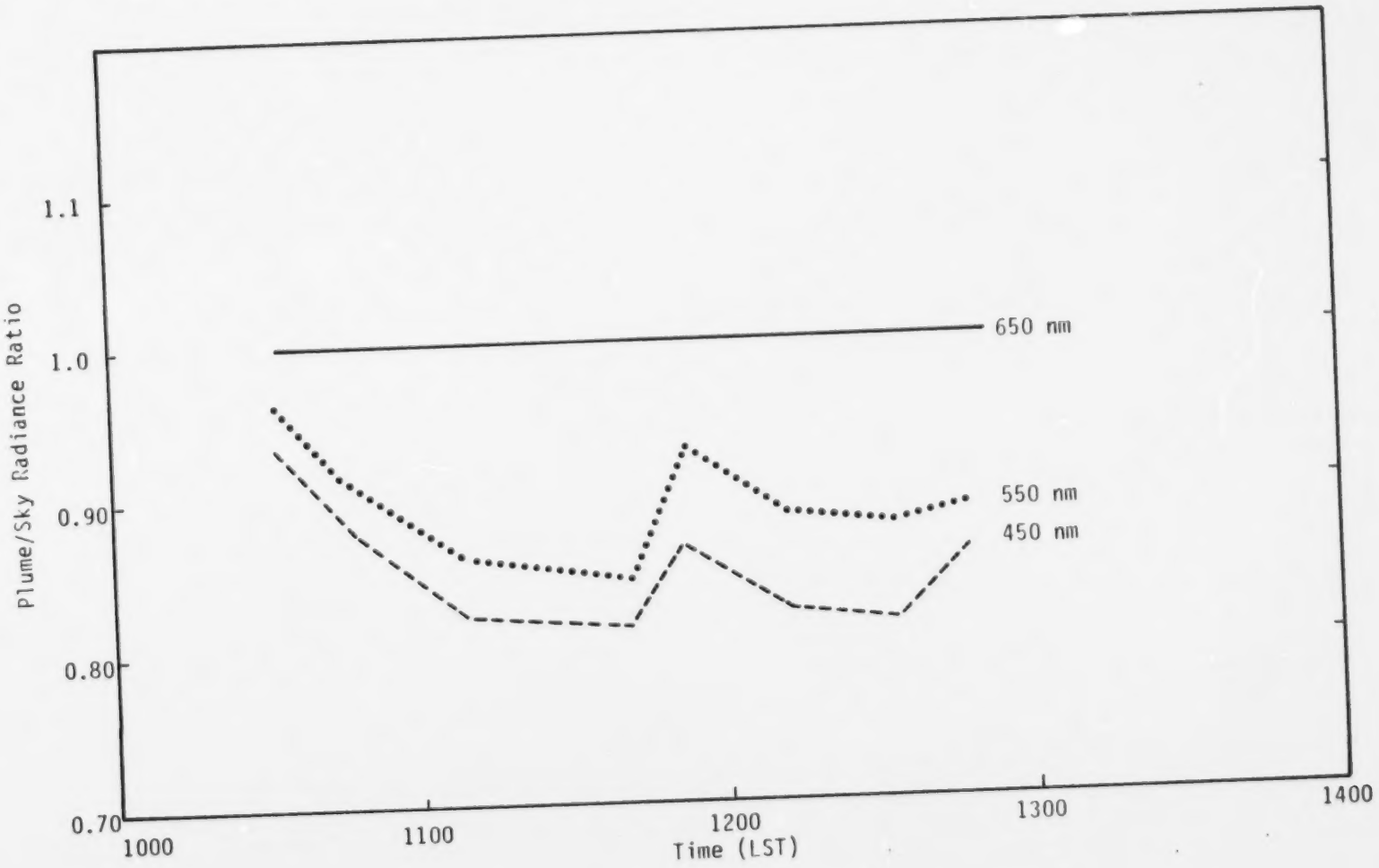

FIGURE 3. Navajo power plant plume. 7 December 1979 (Lechee Rock site).

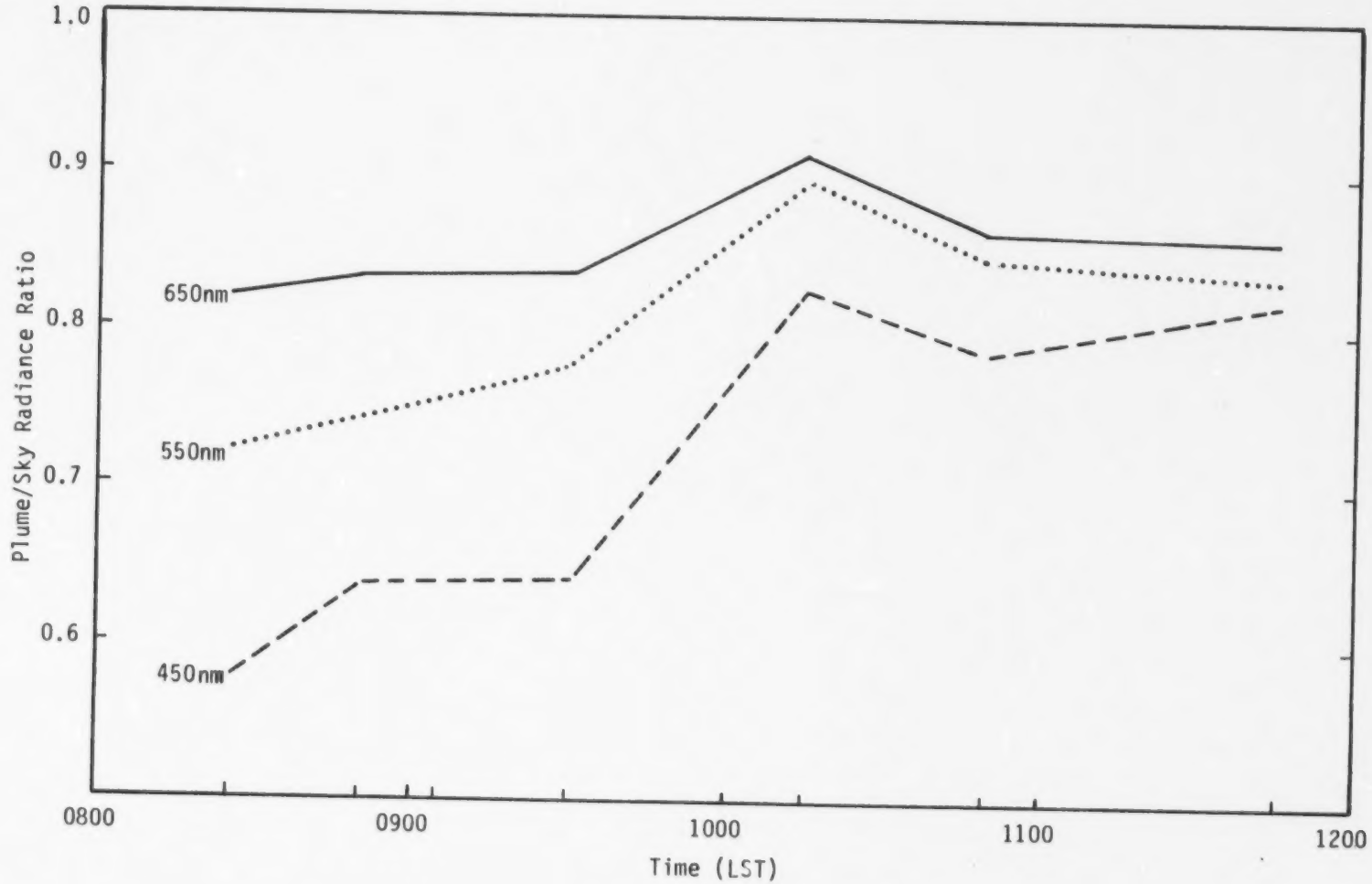

FIGURE 4. Navajo power plant plume. 15 December 1979.

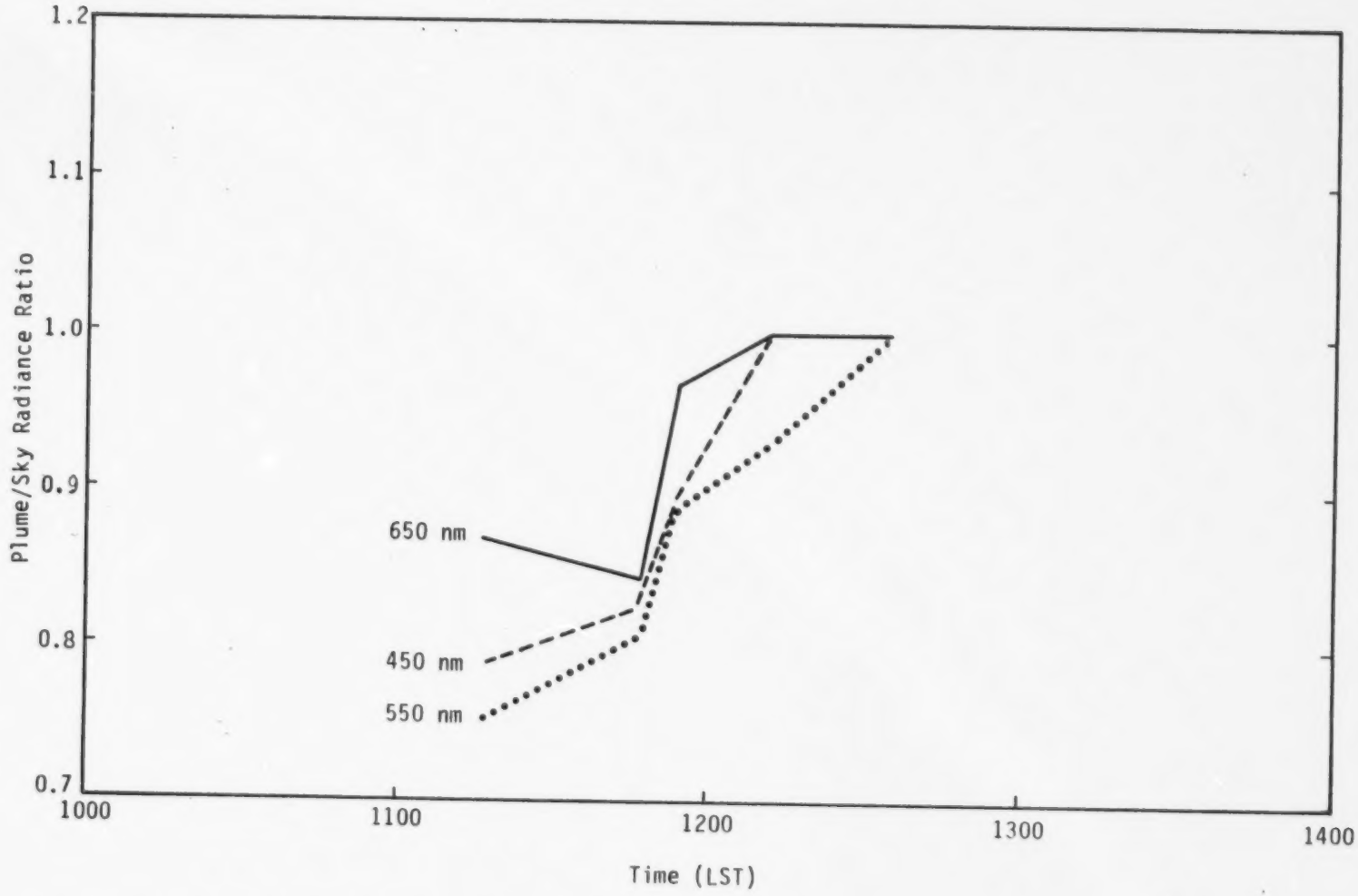

FIGURE 5. Kincaid power plant plume. 20 February 1981.

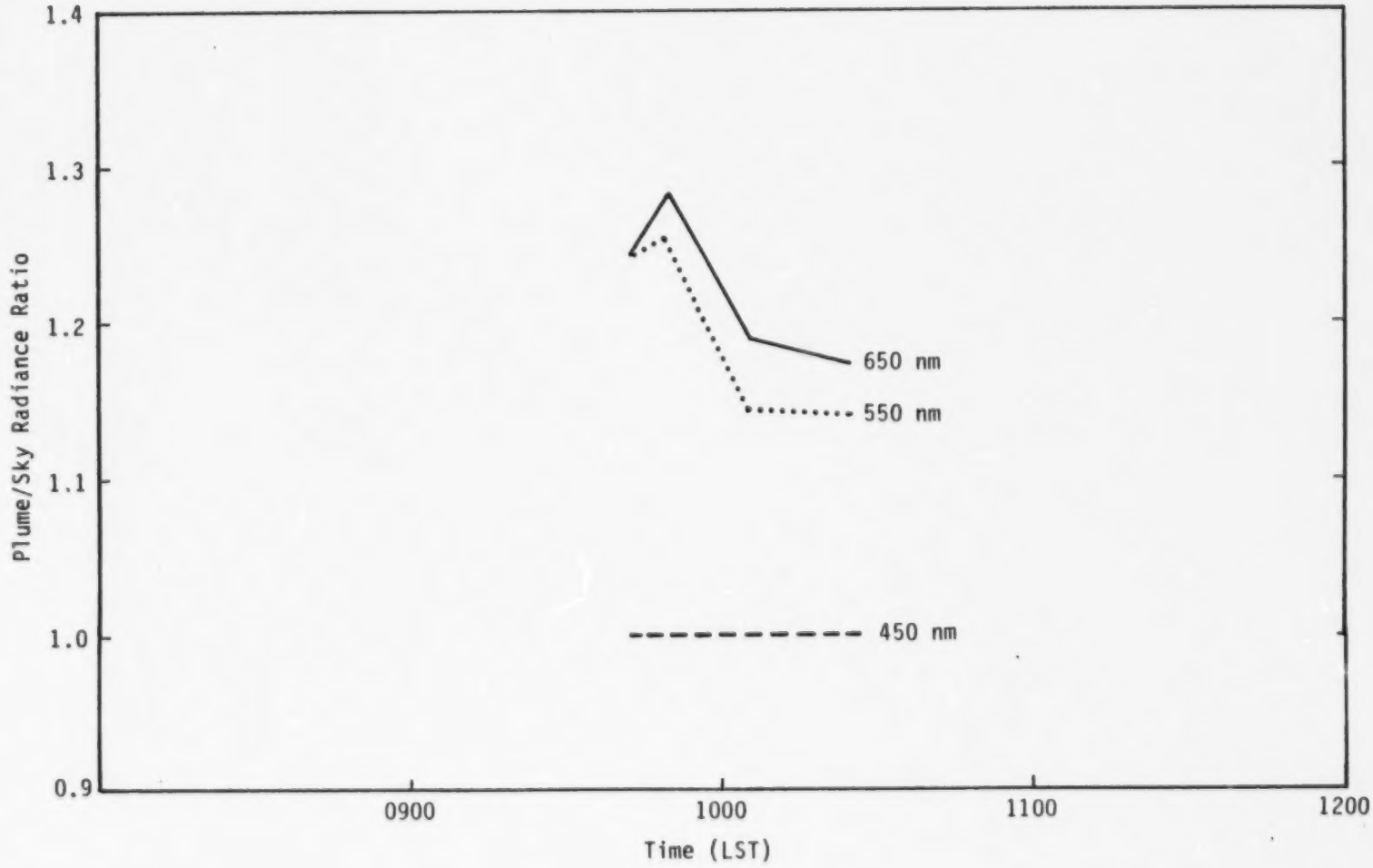

FIGURE 6. Kincaid power plant plume. 24 February 1981 (right side of slide).

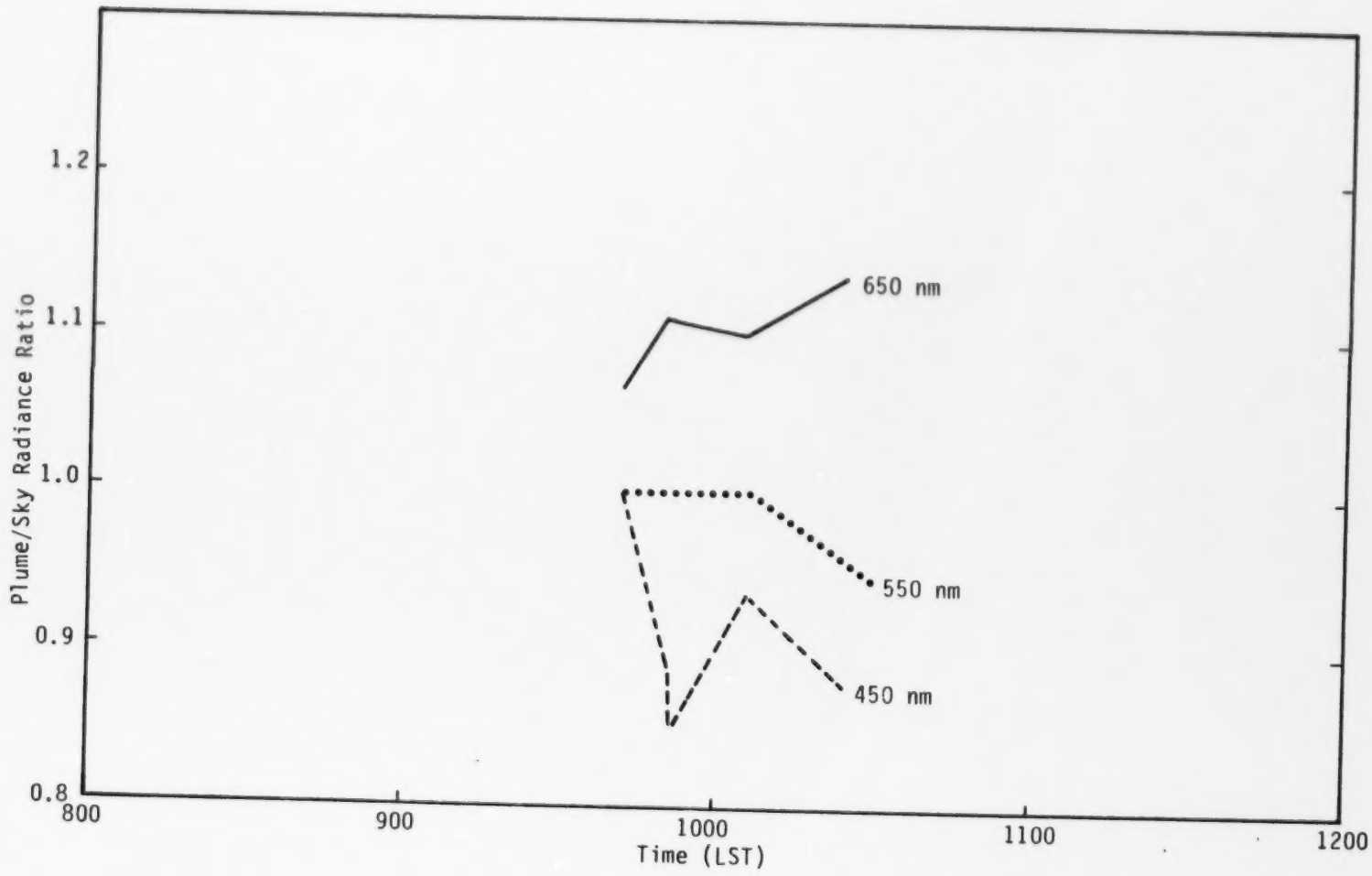

FIGURE 7. Kincaid power plant plume. 24 February 1981 (left side of slide).

changes from stable to less stable. The darkest plume observed during the VISTTA 1979 program (Bergstrom et al., 1981) is reported at 0825 LST in the blue range (a plume/sky radiance ratio of about 0.6). In three hours, this ratio increases to about 0.8. Teleradiometer measurements reported values ranging from 0.83 to 0.90 after 1125 LST (it should be noted that close agreement between sensitometric and teleradiometric measurements should not be expected here since the two sets of measurements may not necessarily correspond to the same portion of the plume). The dispersion of the plume appears fairly constant except for a slight decrease in the plume/sky radiance ratio between 1000 and 1045 LST.

Figure 5 shows the visual effects of the Kincaid power plant plume on 20 February 1981. This case is similar to the previous one, since it shows plume dispersion leading to a net decrease in the plume contrast (i.e., the plume/sky radiance ratio tends toward 1 as the plume becomes more dispersed). The Kincaid power plant plume contains higher concentrations of particles, which is reflected in a higher value of the blue/red ratio (the ratio of plume/sky radiance ratio at the blue and red wavelengths) than for the Navajo power plant plume. The plume visual effects appear to be larger at the green wavelengths.

Figures 6 and 7 present time series of the Kincaid power plant plume observed on 24 February 1981 from the same site but at different azimuth angles, that is to say, the observer is sighting different portions of the plume. This case corresponds to a geometry where the sun is behind the plume and in a forward scattering angle in the right side of the observed plume, and with a backward scattering angle in the left side of the observed plume.

Figure 6 presents the right side of the plume that results in a bright plume due to forward scattering of light by plume particles. Figure 7 presents the left side of the plume that results in a dark plume due to less forward scattering and more backward scattering of aerosols. It may be noted, however, that the plume is still more radiant at the red wavelength in Figure 7; however, it is dark at the green and blue wavelengths. The temporal fluctuations of the plume appear in both figures and show some synchronism. The plume is most discernible around 0945 LST, when it is brighest in Figure 6 and darkest in Figure 7. It is least discernible around 1005 LST, when the plume/sky radiance ratios are closest to 1 in both figures.

Figures 8 and 9 present the results of model simulations of the plume/sky radiance ratio of the Kincaid power plant plume on 24 February 1981 from 0942 to 1024 LST. Figure 8 presents the simulation results that correspond to the right side of the corresponding slides, and Figure 9 presents the simulation results that correspond to the left side of the

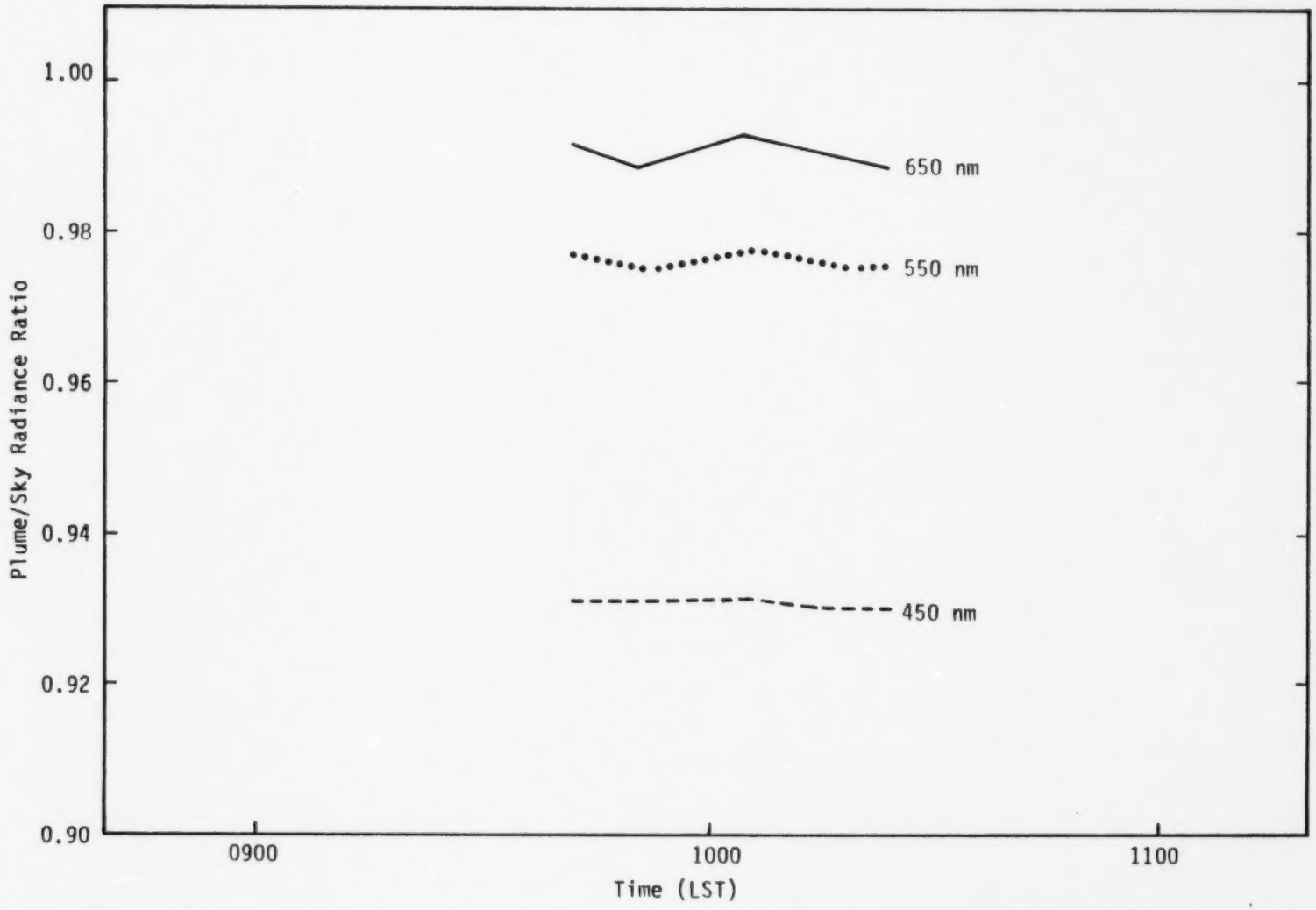

FIGURE 8. Model simulation of the Kincaid power plant plume. 24 February 1981 (right side of slide).

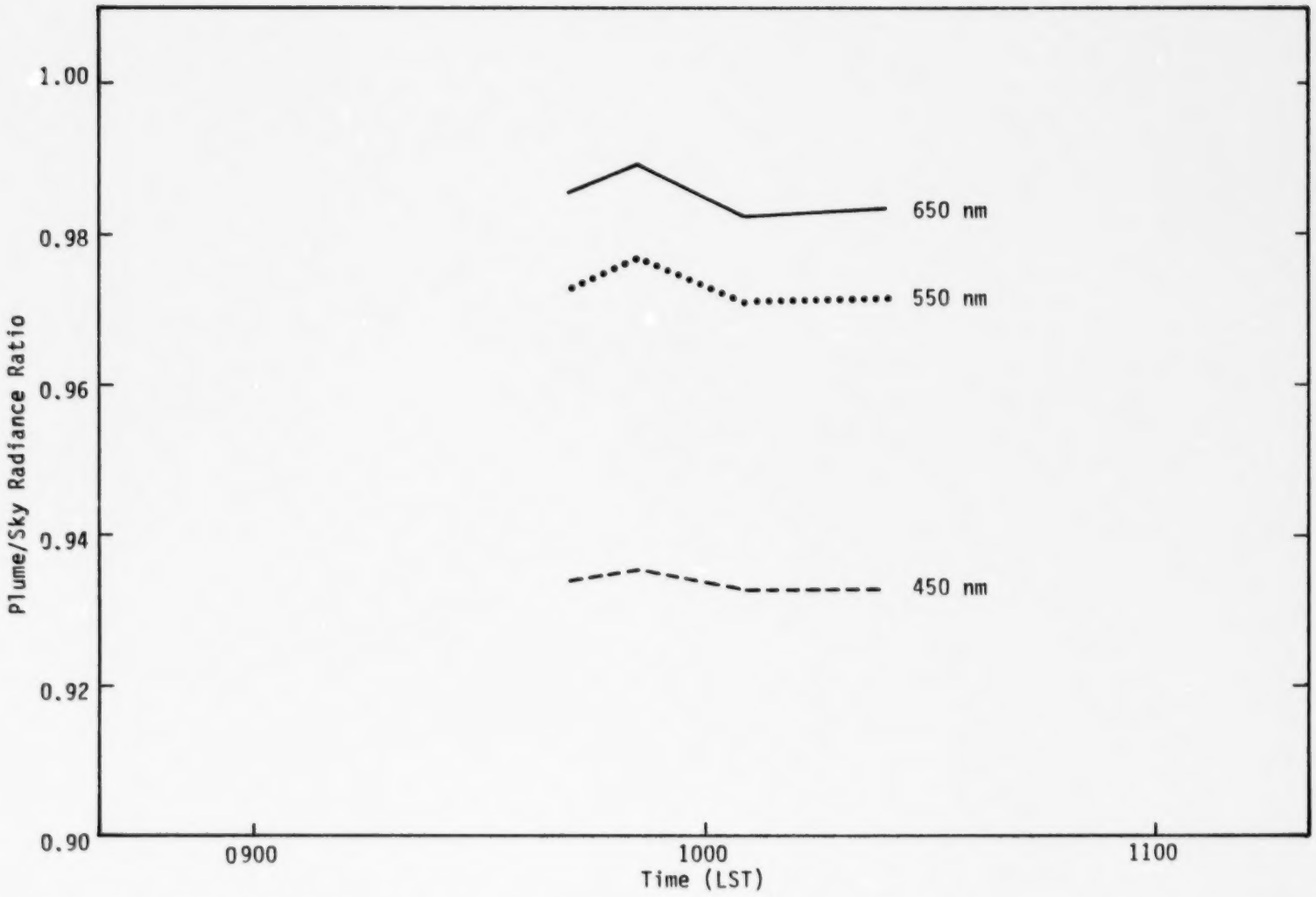

FIGURE 9. Model simulation of the Kincaid power plant plume. 24 February 1981 (left side of slide).

corresponding slides. The simulation results presented in these two figures may therefore be compared to the results of the sensitometric measurements that were presented in Figures 6 and 7.

Comparison of Figures 6 and 8 reveals that the model predicts a dark plume whereas measurements show a bright plume. This model bias has been discussed by Seigneur et al. (1984b) and is investigated further in Section 4. It is interesting to note that model simulations provide less variation in the plume/sky radiance ratio than do measurements. This disparity is to be expected since the model calculation assumes steady-state conditions, and fluctuations due to changes in wind direction, turbulent eddies, and variations in other parameters such as emission rates, visual range, etc., do not appear in the model simulation. The changes in plume-sky radiance ratios calculated by the model result solely from the change in the solar position, i.e., observer-plume-sun scattering angle. Some small fluctuations in the model simulations (Figure 8) result from changes in the scattering angle. In the red and green wavelengths the plume/sky radiance ratio decreases from 0942 LST (scattering angle = 52°) to 0951 LST (scattering angle = 54°); it reaches a maximum value at 1005 LST (scattering angle = 58°) and decreases thereafter until 1024 LST (scattering angle = 62°). Less variation is calculated for the blue wavelength. It may be noted that such trends in the plume/sky radiance ratio are also observed in the sensitometric measurements (Figure 6). For example, at the green and red wavelengths, a peak in the plume/sky radiance ratio occurs around 0951 LST, i.e., a little earlier than in the simulations, and this ratio decreases thereafter. In the blue wavelength little variation occurs and the plume is not visible.

Figure 9 shows a similar pattern. Model calculations also tend to underpredict the value of the plume radiance. Variations are apparent in the plume/sky radiance ratio, with a maximum value at 0951 LST (scattering angle of 75°) for all wavelengths, a minimum value at 1005 LST (scattering angle of 78°), and a slight increase up to 1024 LST (scattering angle of 82°). The variation in the plume sky radiance ratio with time is the reverse of that shown in Figure 8. In Figure 7, the observed plume/sky radiance ratio shows the same trend at the red wavelength, i.e., an increase from 0942 to 0951 LST, a slight decrease from 0951 to 1005 LST, and a final increase up to 1025 LST. Different trends are observed at the green and blue wavelengths.

In summary, it appears that the visual effects of particulate plumes are quite complex because of their dependence on the scattering angle. This complexity is exemplified in the model simulation results (Figures 8 and 9). In addition, atmospheric fluctuations and aerosol characteristics (e.g., size distribution, nonspherical particles) introduce variations (Figures 6 and 7) that are difficult to predict with accuracy.

Our analysis of the temporal variability of plume visibility has shown that notable variation in the plume visual effects occurs as a function of time. These variations, which exceed the uncertainties of the sensitometric measurements, may represent

(1) An evolution of atmospheric stability toward more unstable conditions that lead to a more dispersed and less discernible plume.

(2) A variation in plume visual effects that results from a change in the scattering angle and the associated varying effects of particulate scattering.

These variations may also occur in a random manner and may represent atmospheric turbulent fluctuations that are reflected in nonstationary characteristics of the plume.

5 SPATIAL VARIABILITY OF PLUME VISIBILITY

The ratios of plume radiance to sky radiance were calculated by the sensitometric technique and plotted for each of the four case studies analyzed (see Table 2) as a function of the observed azimuth angle, i.e., as a function of the horizontal distance along the color slide. The results of these analyses are presented in Figures 10 through 13. The plume/sky radiance ratio is presented for three wavelengths--450, 550 and 650 nm.

Figure 10 presents the results of the Navajo power plant plume photographed at 1200 LST on 7 December 1979. It appears that the plume is clearly well defined at all the azimuths. At 450 nm, for example, the plume is darker on the right side of the color slide (ratio of 0.75) than on the left side (ratio of 0.8). This finding is consistent with the fact that the power plant plume is dispersing from the right toward the left, and the plume should therefore be more dilute on the left than on the right.

Figure 11 presents the results of the Navajo power plant plume observed on 15 December 1979 at 0905 LST. This graph presents a clear example of the evolution of plume visual effects with downwind distance. The plume/sky radiance ratios on the right side (i.e., closest to the stacks) are 0.6, 0.73, and 0.82 for 450 nm, 550 nm, and 650 nm, respectively. The wavelength distribution is characteristic of an NO_2-laden plume with little particulate matter. As the plume is transported downward, it becomes more dilute; the plume/sky radiance ratios on the left side are 0.66, 0.78, and 0.92 at 450, 550, and 650 nm, i.e., larger than on the right side of the plume. The evolution of the visual effects of the plume appears to be fairly continuous, and fluctuations that appear on the graph may be due to atmospheric fluctuations but are close to the values of the uncertainties associated with sensitometric measurements.

Figure 12 presents the plume/sky radiance ratios at 450, 550, and 650 nm for the Kincaid power plant plume on 20 February 1981 at 1117 LST. The plume presents nearly constant visual effects across the azimuth line. However, some variations in the plume/sky radiance ratio are observed, e.g., in the center of the graph for the blue and green wavelengths. These fluctuations in the ratio are on the order of 0.05, which is

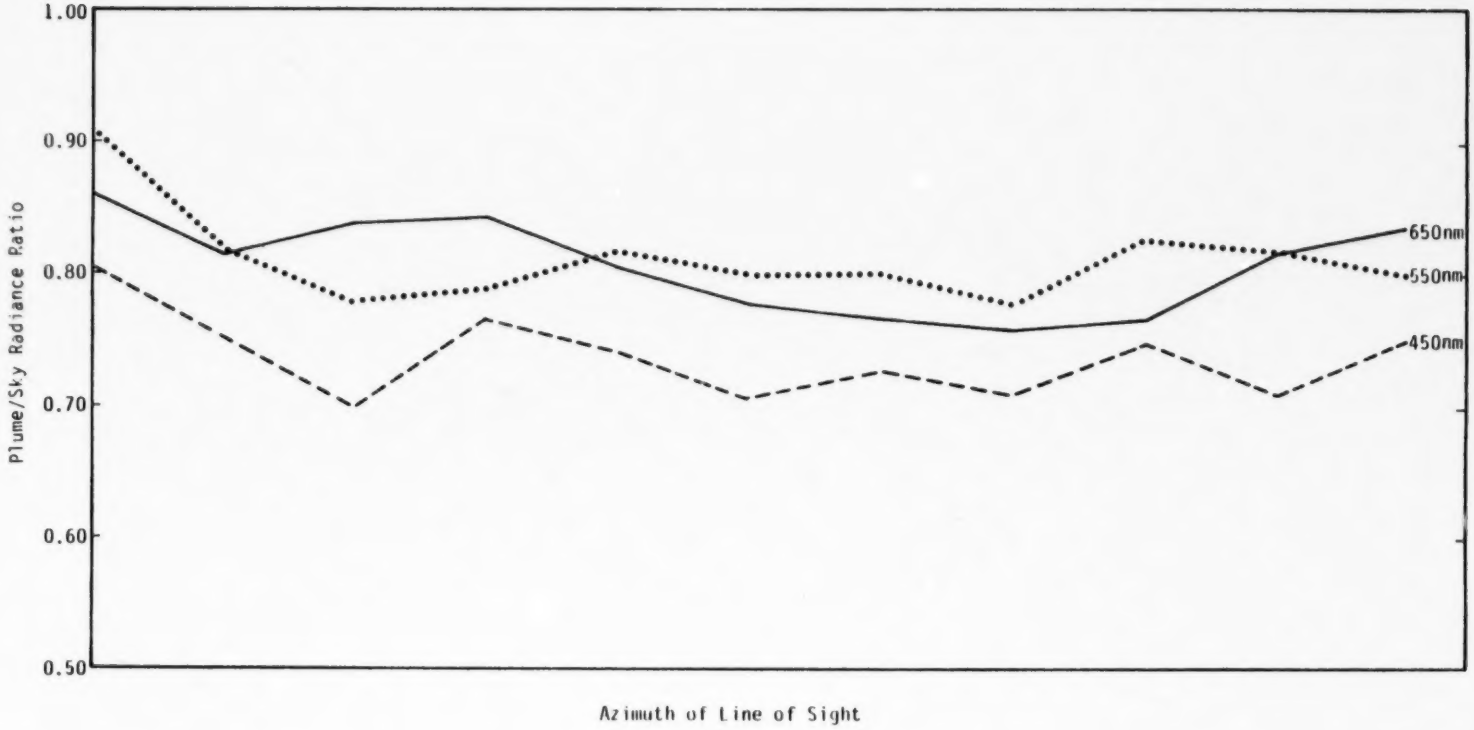

FIGURE 10. Navajo power plant plume. 1200 LST. 7 December 1979.

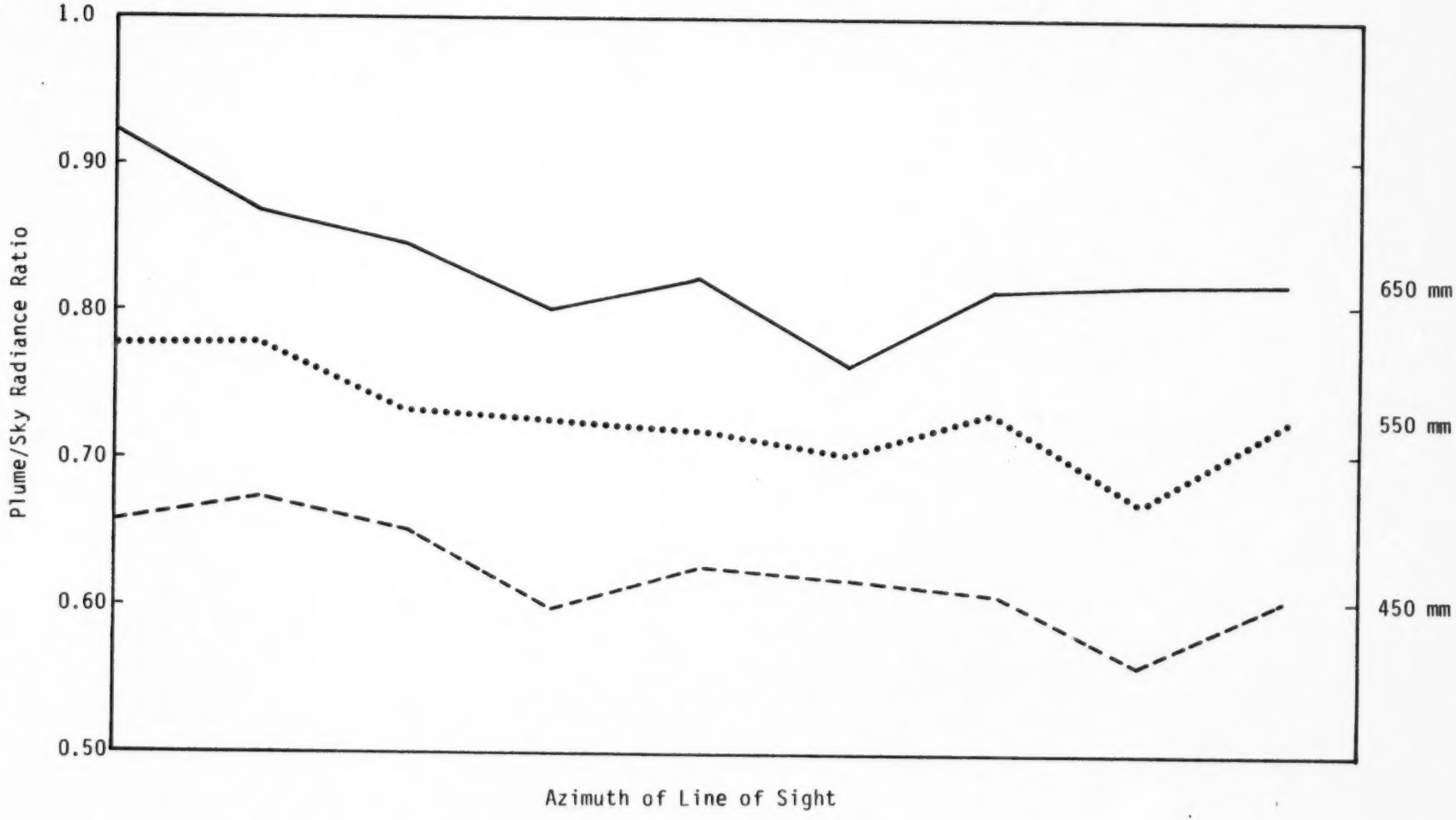

FIGURE 11. Navajo power plant plume. 0905 LST. 15 December 1979.

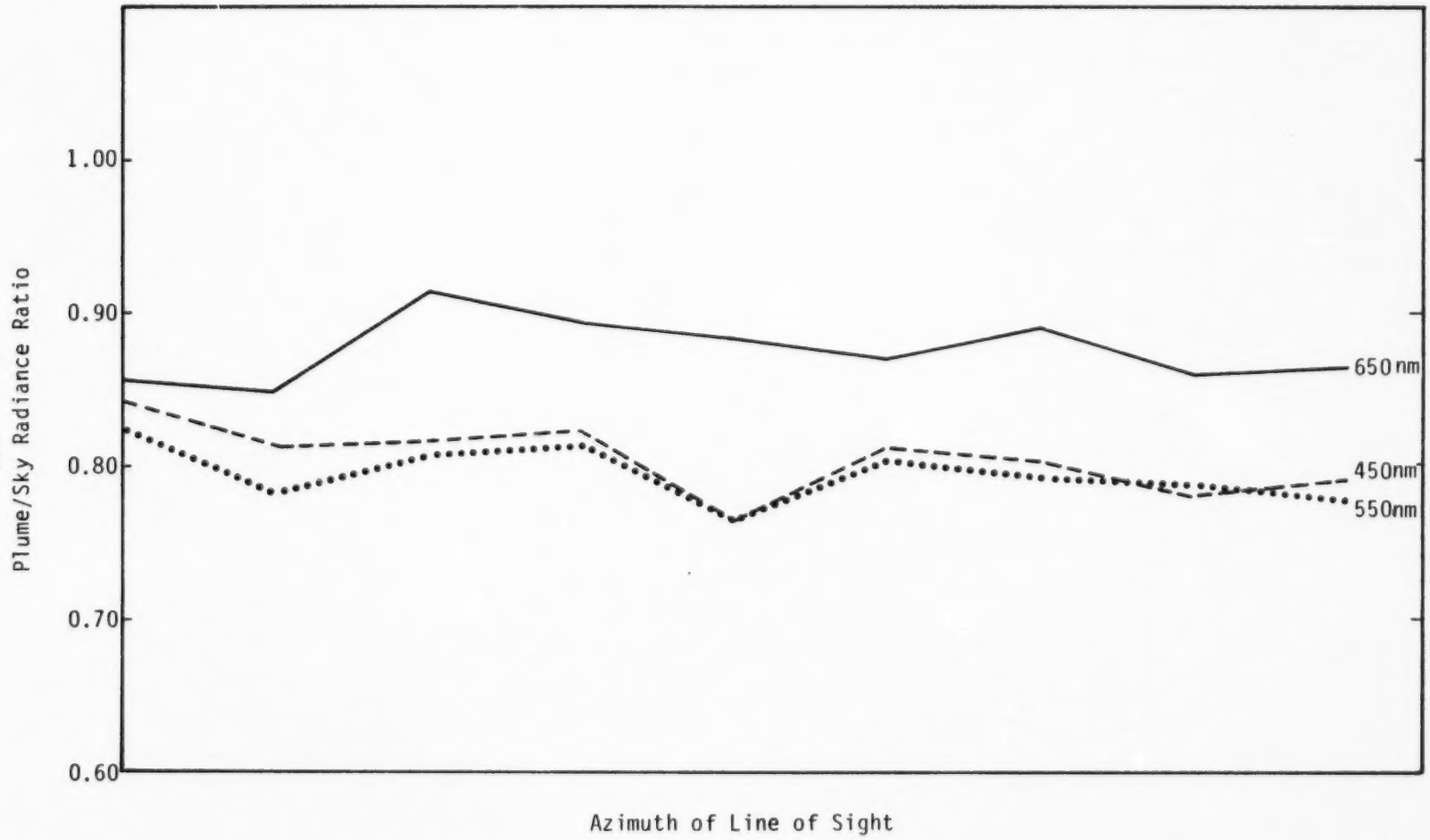

FIGURE 12. Kincaid power plant plume. 1117 LST. 20 February 1981.

slightly larger than the sensitometric measurement uncertainties(4 percent at 0.80 corresponds to 0.03); therefore, these fluctuations are likely to be due to actual spatial variations in the plume visual effects.

Figure 13 presents the plume/sky radiance ratio for the Kincaid power plant plume photographed on 24 February 1981 at 0951 LST. This case study is particularly interesting because it presents a bright plume on the right side of the photograph, where forward scattering is important, and a dark plume on the left side of the photograph, where backward scattering begins to dominate. The visual aspects of the plume in the color slide are quantitatively revealed on this graph. On the right side, forward scattering of plume particles leads to plume/sky radiance ratios greater than 1 (bright plume) at 550 and 650 nm, and no effect is apparent at the blue wavelength. On the left side, scattering by the plume particles reduces the plume radiance notably in the blue wavelength. There is still some significant amount of forward scattering by plume particles at the red wavelength. The difference in the plume visual effects between the right and left sides is fairly monotonic and results primarily from the change in scattering angle. However, some fluctuations are observed at the red wavelength toward the center of the graph.

Figure 14 presents the results of a model simulation of the plume/sky radiance ratio for the Kincaid power plant plume on 24 February 1981 at 0951 LST. The azimuth of the line of sight corresponds to that of the photograph; therefore, Figure 14 can be compared with Figure 13. As noted in Section 3 in the discussion of Figures 8 and 9, the model underestimates the plume radiance relative to the background radiance.

The general trend of lower plume/sky radiance ratios at the left side of the slide and higher plume/sky radiance ratios at the right side of the slide is apparent in the model simulation for the red and green wavelengths. The variations in the plume/sky radiance ratios are not monotonic; the ratios increase from the left side of the slide (scattering angle of 85°), and local maxima are attained toward the left side of the slide (scattering angle of 75°). The ratios then decrease to reach local minima near the center of the slide (scattering angle of 65°), and continue to decrease at the blue wavelength but increase at the red and green wavelengths toward the right of the slide (scattering angle of 50°).

These results can be compared with those presented in Figure 13. The same pattern is obtained for the red wavelength in both the model simulation and the measurements, with a sequence of increase, decrease, and increase in the plume/sky radiance ratio from the left to the right. The trend is not as pronounced at the green wavelength. At the blue wavelength, no notable variation is observed in the right half of the slide, whereas the model simulation shows a decrease in the plume/sky radiance ratio.

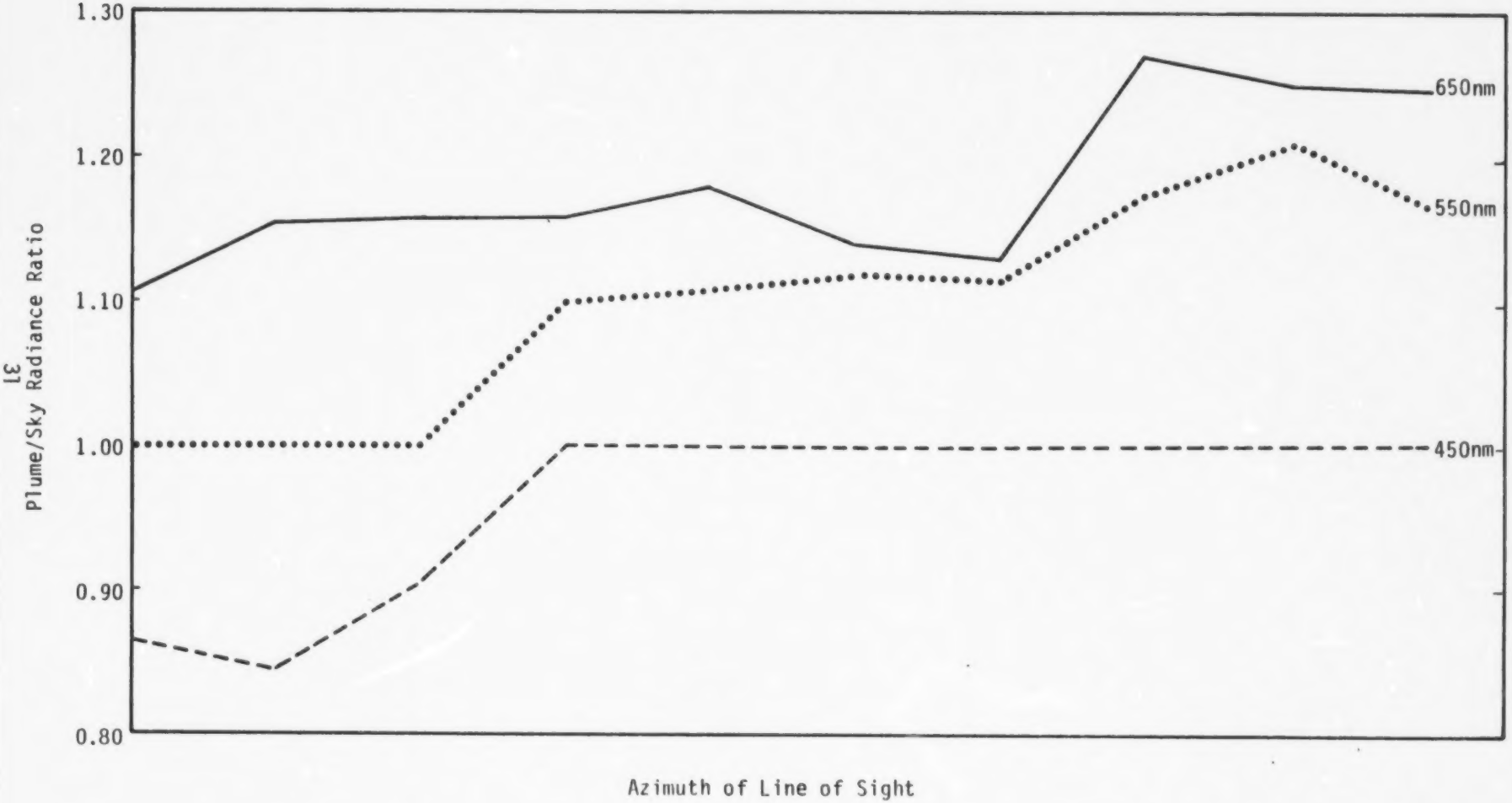

FIGURE 13. Kincaid power plant plume. 0951 LST. 24 February 1981.

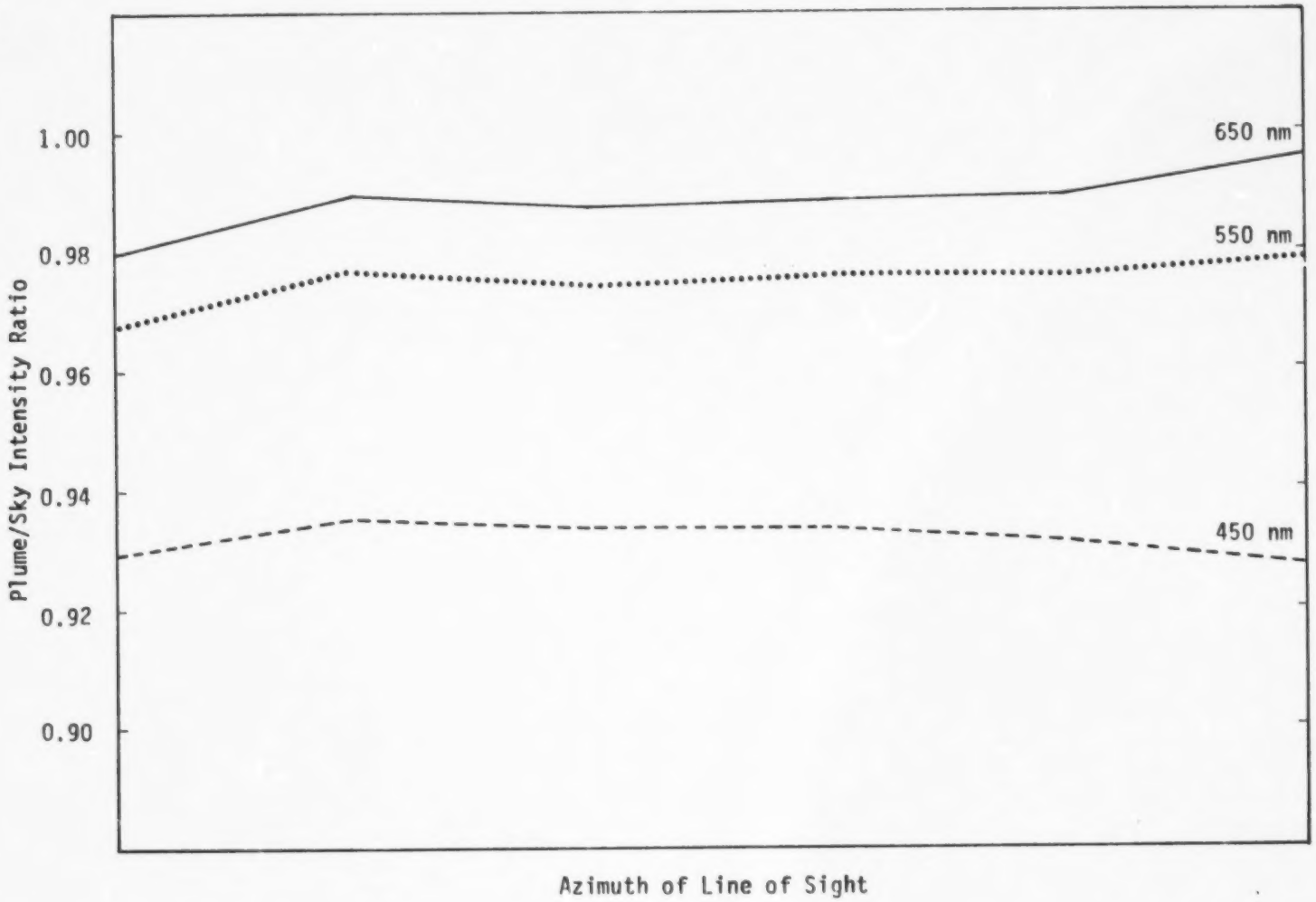

FIGURE 14. Model simulation of the Kincaid power plant plume. 0951 LST. 24 February 1981.

We investigated the sensitivity of the plume model visibility calculations to two parameters--wind direction and aerosol size distribution--that affect the scattering properties of the plume.

In the first simulation, the wind direction was changed from 330° to 340°; this variation results in a change in the scattering angles by 1° (left side of the slide) to 5° (right side of the slide). The results of the model simulation are presented in Figure 15. It appears that a small change in wind direction (10°) leads to small changes in scattering angle (less than 5°) and therefore has little effect on the calculated plume/sky radiance ratio.

In the second simulation, the mean radius of coarse aerosols was changed from 3.4 to 5 μm. Because light scattering by aerosols depends on their size, this change in the aerosol size distribution should lead to changes in light scattering by the plume. The results of the model simulations are presented in Figure 16. It appears that only small changes result from this different aerosol size distribution, for example, the plume/sky radiance ratio increases from 0.980 to 0.982 at the left side of the slide and decreases from 0.995 to 0.990 at the right side of the slide. However, these variations cannot account for the bias of the model toward underprediction of the plume/sky radiance ratio.

These sensitivity model calculations show the dependence of the plume scattering properties on the observer-plume-sun scattering angle and on the aerosol size distribution. However, variations in these input parameters that are commensurate with the experimental uncertainties do not explain the bias of the model simulations. This matter was investigated further by conducting a sensitivity analysis of the optics component of the plume visibility model for this particular case study.

We used the aircraft data as input to the optics component of the plume visibility model to simulate the plume at 0814 LST, the time corresponding to the field measurements (Seigneur et al., 1984b). The plume visibility model calculates the formation of fine aerosols in the plume due to sulfate formation and assumes that all emitted (primary) aerosols are in the coarse mode. For this particular case study, the PLUVUE II model calculated that no significant fine aerosol formation occurred and the plume aerosol was therefore concentrated in the coarse mode. Comparison of the plume optics calculations with the measurements did not show any improvement over the plume model calculation since a dark plume was still predicted (Seigneur et al., 1984b).

Analysis of the plume aerosol size distribution showed that plume aerosols were present in both the fine and the coarse modes (Richards et al., in

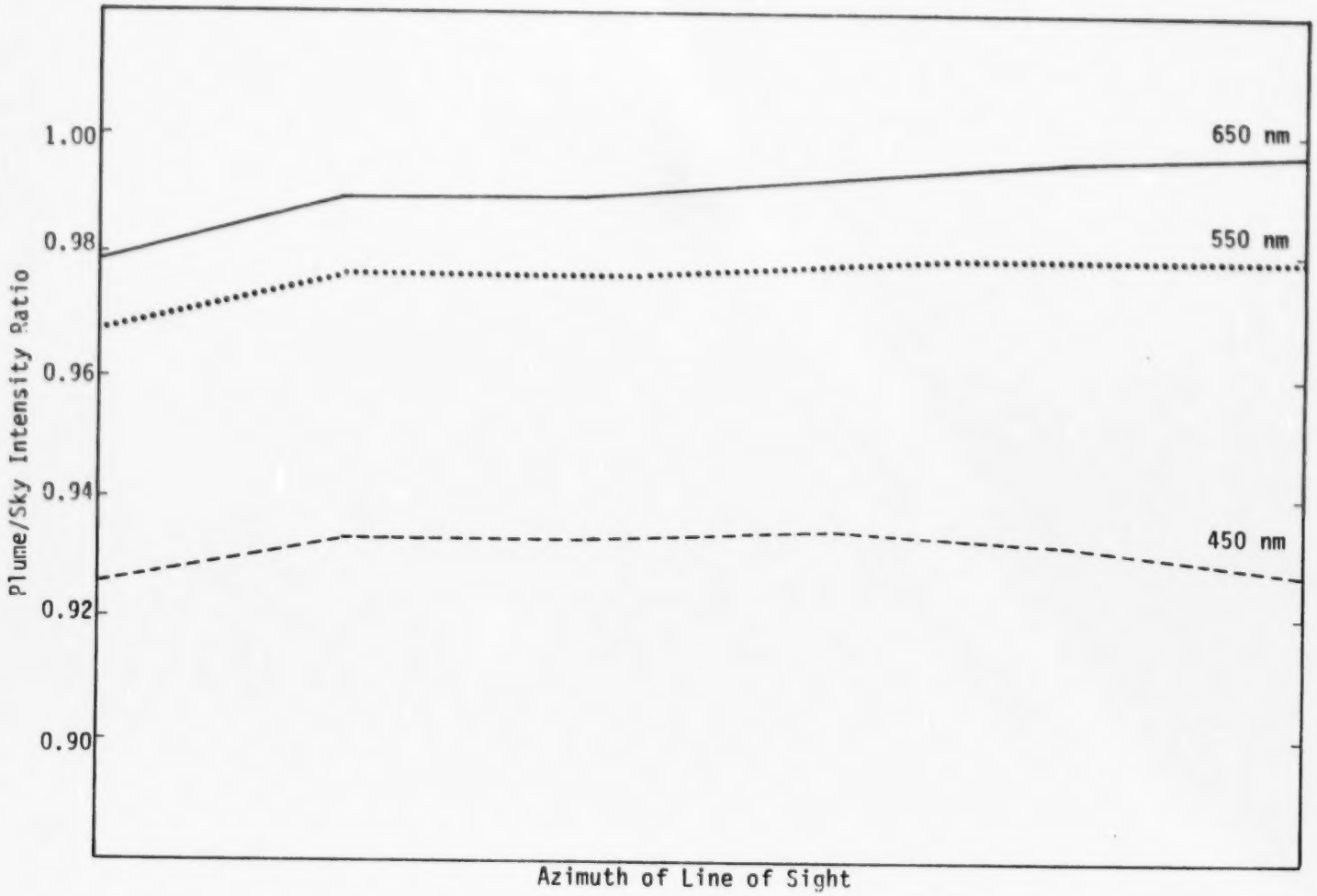

FIGURE 15. Model simulation of the Kincaid power plant plume. 0951 LST. 24 February 1981. Wind direction = 340°.

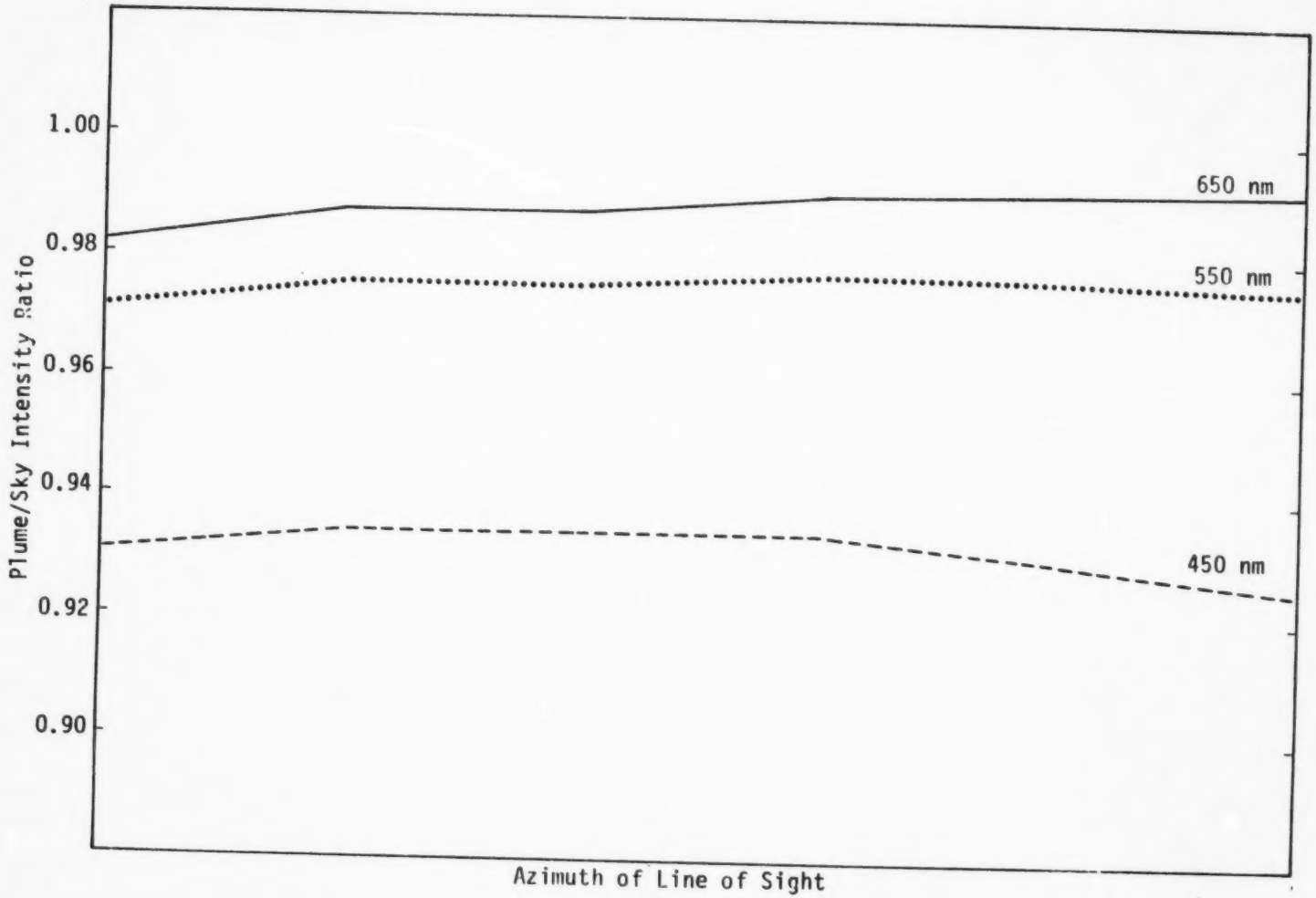

FIGURE 16. Model simulation of the Kincaid power plant plume. 0951 LST. 24 February 1981. Mean radius of coarse aerosols = 5 μm.

press). Consequently, we investigated the effect of these fine aerosols on the plume optics calculations. We performed these calculations with 50 percent, 33 percent, 67 percent, and 100 percent of fine aerosols, the rest consisting of primary (coarse) aerosols. (The original plume optics calculation involved 100 percent of primary aerosols.) In all these simulations, the aerosol mass was selected to ensure that the calculated b_{scat} coefficients matched the measured value.

The results of these calculations are presented in Table 3. It appears that the presence of fine aerosols leads to a bright plume in the model calculations, although the wavelength dependence of the plume/sky radiance ratio is not as strong as in the reported measurements. These fine aerosols may result from either emission of fine aerosols or formation of sulfate aerosols in the plume. The PLUVUE and PLUVUE II models do not treat emission of fine aerosols and simulate sulfate formation in the plume according to a clean air chemical mechanism that may not apply to the Kincaid environment. The inability to treat emissions of fine aerosols in the PLUVUE and PLUVUE II models should be rectified, based on this case study.

Our analysis of the spatial variability of plume visibility has shown that variations in the plume visual effects occur as the azimuth of the observer's line of sight changes. These variations exceed the uncertainties of the sensitometric measurements and may occur in a monotonic form, representing either

(1) A decrease in plume visual effects due to dilution of the plume and/or increase in the observer/plume distance, or

(2) A variation in plume visual effects (e.g., from bright to dark plume) that results from a change in the scattering angle and the associated varying effects of particulate scattering.

They may also occur in a random manner, representing atmospheric turbulent fluctuations that lead to nonhomogeneous characteristics of the plume.

TABLE 3. Comparison of measured and calculated plume/sky radiance ratios for the Kincaid power plant plume, 0814 LST, 24 February 1981.

Wavelength (nm)	Plume/Sky Radiance Ratio					
		PLUVUE II Optics Component				
		Aerosol Distribution				
	Teleradiometer Measurements	100 Percent Coarse	67 Percent Coarse 33 Percent Fine	50 Percent Coarse 50 Percent Fine	33 Percent Coarse 67 Percent Fine	100 Percent Fine
405	1.02	0.94	1.00	1.03	1.05	1.10
450	1.04	0.94	1.00	1.03	1.06	1.11
550	1.10	0.98	1.01	1.04	1.06	1.11
630	1.15	1.00	1.02	1.04	1.06	1.11

REFERENCES

Bergstrom, R. W., C. Seigneur, B. L. Babson, H. Y. Holman, and M. A. Wojcik. 1981. Comparison of the observed and predicted visual effects caused by power plant plumes. Atmos. Environ., 15:2135-2150.

Blumenthal, D. L., L. W. Richards, E. S. Macias, R. W. Bergstrom, W. E. Wilson, and P. S. Bhardwaja. 1981. Effects of a coal-fired power plant and other sources on southwestern visibility (interim summary of EPA's project VISTTA). Atmos. Environ., 15:1955-1970.

Eastman Kodak Company. 1974. Sensitometric and Image Structure Data--Kodachrome 64 Film (Daylight). Eastman Kodak Company, Rochester, New York (E-78-8).

Eastman Kodak Company. 1976. Kodak Filters for Scientific and Technical Uses. Eastman Kodak Company, Rochester, New York (0-87985-029-9).

Macbeth. 1981. The Macbeth Color Checker. Macbeth, Newburgh, New York.

Richards, L. W., J. A. Anderson, D. L. Blumenthal, A. A. Brandt, J. A. McDonald, N. Waters, E. S. Macias, and P. S. Bhardwaja. 1981. The chemistry, aerosol physics, and optical properties of a western coalfired power plant plume. Symposium on Plumes and Visibility: Measurements and Model Components, 10-14 November 1980, Grand Canyon, Arizona. Atmos. Environ., 15:2111-2134.

Richards, L. W., J. A. Anderson, D. L. Blumenthal, J. A. McDonald, E. S. Macias, S. V. Hering, and W. E. Wilson, Jr. In press. Chemical, aerosol, and optical measurements in the plumes of three midwestern coal-fired power plants. Atmos. Environ.

Seigneur, C., H. Hogo, and C. D. Johnson. 1984a. Comparison of teleradiometric and sensitometric techniques for visibility measurements. Atmos. Environ., 18:227-233.

Seigneur, C., R. W. Bergstrom, C. D. Johnson, and L. W. Richards. 1984b. Measurements and simulations of the visual effects of particulate plumes. Atmos. Environ., 18:2231-2244.

White, W. H., C. Seigneur, D. W. Heinold, M. W. Eltgroth, L. W. Richards, P. T. Roberts, P. S. Bhardwaja, W. D. Connor, and W. E. Wilson. In press. Predicting the visibility of chimney plumes: an intercomparison of four models with observations at a well-controlled power plant. Atmos. Environ.